Inorganic Chemistry
Cite This: Inorg. Chem. XXXX, XXX, XXX–XXX
Article
pubs.acs.org/IC

Iron-Catalyzed/Mediated C–N Bond Formation: Competition between Substrate Amination and Ligand Amination

Suman Sinha,[†,#] Rina Sikari,[†,#] Vivek Sinha,[‡,¶] Upasona Jash,[†] Siuli Das,[†] Paula Brandão,[§] Serhiy Demeshko,[⊥] Franc Meyer,[⊥] Bas de Bruin,[‡] and Nanda D. Paul*[,†]

[†]Department of Chemistry, Indian Institute of Engineering Science and Technology, Shibpur Botanic Garden, Howrah 711103, India

[‡]Homogeneous Catalysis Group, van't Hoff Institute for Molecular Sciences, University of Amsterdam, Science Park 904, 1098 XH Amsterdam, The Netherlands

[§]Departamento de Química, CICECO-Instituto de Materiais de Aveiro, Universidade de Aveiro, 3810-193 Aveiro, Portugal

[⊥]Universität Göttingen, Institut für Anorganische Chemie, Tammannstrasse 4, D-37077 Göttingen, Germany

Supporting Information

ABSTRACT: Iron catalyzed carbon–nitrogen bond formation reactions of a wide variety of nucleophiles and aryl halides using well-defined iron-complexes featuring redox noninnocent 2-(arylazo)-1,10-phenanthroline (L^1) ligands are reported. Besides substrate centered C–N coupling, C–N bond formation reactions were also observed at the *ortho*- and *para*-positions of the phenyl ring of the coordinated azo-aromatic scaffolds affording new tetradentate ligands, 2-N-aryl-(2-arylazo)-1,10-phenanthroline (L^2), and tridentate ligands, 4-N-aryl-(2-arylazo)-1,10-phenanthroline (L^3), respectively. Control experiments and mechanistic studies reveal that the complex $[FeL^1Cl_2]$ (**1**) undergoes in situ reduction during the catalytic reaction to produce the monoanionic complex $[\mathbf{1}]^-$, which then acts as the active catalyst. The metal (iron) and the coordinated ligand were found to work in a cooperative manner during the transfer processes involved in the fundamental steps of the catalytic cycle. Detailed experimental and theoretical (DFT) studies were performed to get insight into the competitive substrate versus ligand centered amination reactions.

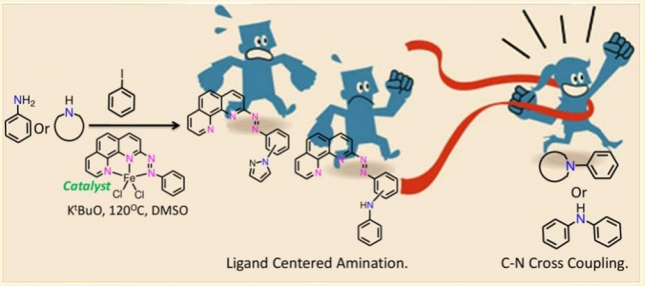

INTRODUCTION

Construction of C–N bonds is one of the important challenges in organic synthesis due to the widespread presence of nitrogen-containing compounds in a broad spectrum of synthetic and natural organic molecules.[1] Notable progress has been made in developing catalytic and stoichiometric C–N bond forming reactions. Numerous synthetic methods including both metal catalyzed and classical organic reactions were developed for carbon–nitrogen bond formation via direct functionalization of C–X (X: H, halides, pseudo halides, etc.) bonds.[2−6] However, most of the metal catalyzed C–N bond formation reactions were successfully achieved using the scarce and relatively expensive noble metal based catalysts such as palladium,[3] rhodium,[4] or ruthenium.[5] Therefore, achieving C–N cross coupling reactions using cheap and easily accessible catalysts based on 3d-base metals is desirable.

Consequently, worldwide extensive research efforts are undertaken to develop new strategies for the formation of C–N bonds using cheap and earth abundant base metals as alternatives to the expensive heavy metals like palladium, rhodium, or ruthenium. However, base metals tend to undergo one-electron oxidation changes, and the subsequent two-electron transfer processes are mostly thermodynamically unfavorable and hence require elevated temperatures. For example, several reported C–N coupling reactions, catalyzed by earth-abundant and cheap Cu and Ni-catalysts, require high temperatures for the reaction to proceed.[6,7] It is worth mentioning here that copper catalysts are very efficient and even produce the desired C–N coupled products in high yield with ppm level catalyst loading.

In this perspective, the catalytic applications of transition metal complexes featuring redox noninnocent scaffolds are of growing interest.[8] Redox noninnocent ligands, other than offering coordination to transition metal ions, can participate in electron transfer processes during different elementary steps of any chemical transformations and thus enable the catalyst to avoid high energy metal centered redox events.[8] In recent times, Chirik and co-workers reported several catalytic reactions such as hydroboration, hydrosilylation, cycloaddition using base metal complexes of redox noninnocent bis(imino)-pyridine ligands. Both metal and the coordinated bis(imino)-

Received: October 10, 2018

DOI: 10.1021/acs.inorgchem.8b02877
Inorg. Chem. XXXX, XXX, XXX–XXX

pyridine ligands were found to participate in a cooperative manner during these catalytic reactions (Scheme 1).[9] Using

Scheme 1. Different Chemical Transformations Using Iron Complexes of Redox Noninnocent Ligands

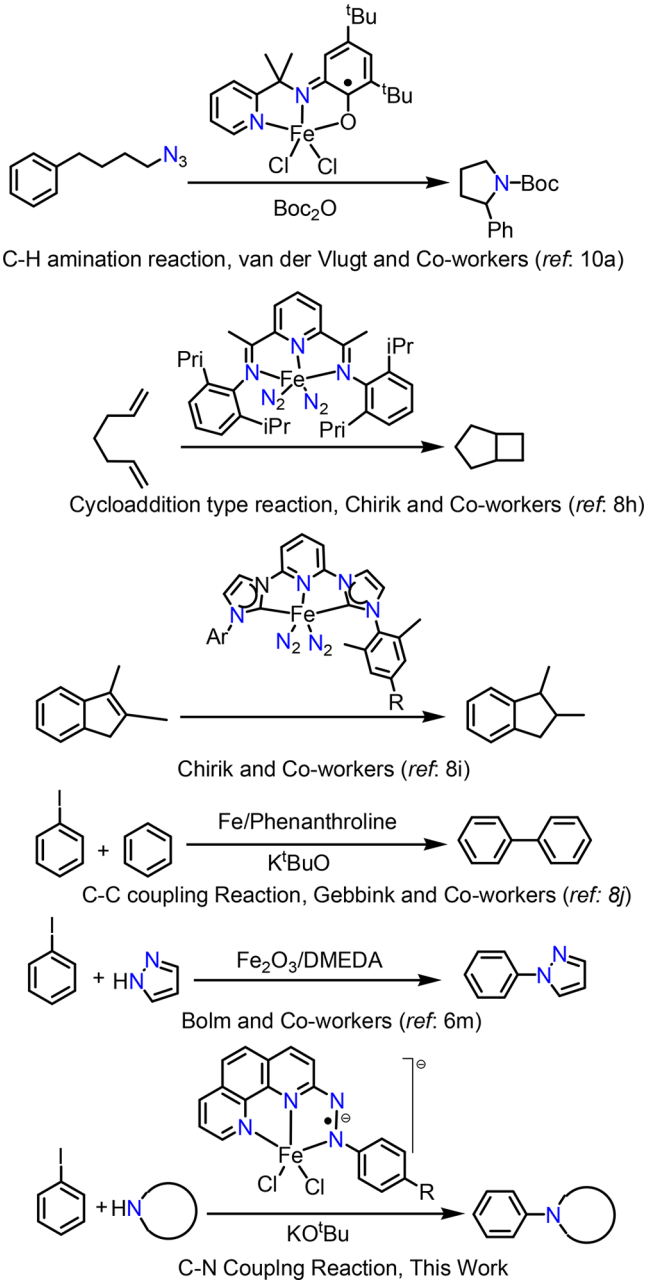

the redox noninnocent properties of diamine and aminophenol based ligand systems, several new catalytic and stoichiometric reactions were explored.[10] Using redox noninnocent carbene radical ligands, de Bruin and co-workers reported several cobalt-catalyzed chemical transformations.[11]

In contrast to the above-mentioned redox noninnocent ligand systems, the application of redox noninnocent azo-aromatic scaffolds in catalysis has been less studied even though their rich redox chemistry has been well established since long.[12] Because of the presence of vacant acceptor orbitals, this class of ligands can accept multiple electrons in their π^* orbitals and thus can act as electron reservoir during catalytic reactions. Only in recent times, Goswami and co-workers reported catalytic alcohol oxidation reactions using nickel and zinc complexes featuring 2,6-bis(phenylazo)pyridine ligands as catalysts. The coordinated 2,6-bis(phenylazo)-pyridine scaffold functions as an electron reservoir in these dehydrogenation reactions.[13]

Recently, we reported the synthesis and characterization of new redox active ligands, 2-(arylazo)-1,10-phenanthroline ($\mathbf{L^1}$) and their iron complexes.[14a] Out of these Fe(II)-complexes reported, the one electron reduced penta-coordinated complexes, $[Fe^{II}\{(L^{1a,b})^{\bullet-}\}Cl_2]^-$ ($[\mathbf{1a}]^-$, $[\mathbf{1b}]^-$) were found to catalyze alcohol oxidation reactions. The coordinated 2-(arylazo)-1,10-phenanthroline ($\mathbf{L^1}$) scaffold as well as the iron-center was found to act in a synergistic manner during the catalytic reaction.[14a] In accordance to our current research to study new catalytic reactions using transition metal complexes of redox noninnocent ligands, we chose the one electron reduced penta-coordinated Fe(II)-complexes $[Fe^{II}\{(L^{1a\text{-}c})^{\bullet-}\}Cl_2]^-$ ($[\mathbf{1a\text{-}c}]^-$) as catalysts to study catalytic C–N bond formation reactions between aryl halides and nitrogen nucleophiles (Scheme 2). Our intention was to (partly) use the ligand centered redox events during the catalytic turnover and thereby to avoid high-energy Fe-centered redox steps during different elementary steps of the catalytic reaction. Two new Fe(III)-complexes $[Fe^{III}L^{a/b}Cl_3]$ (**2a**, **2b**) were synthesized and also employed as catalyst to study the C–N coupling reactions. The low-cost and environmentally benign nature of iron further intrigued us to take up this work.

Interestingly, other than the desired substrate centered amination, competitive C–N bond formation was also observed at the *ortho*- and *para*-positions of the coordinated azo-aromatic ligands ($\mathbf{L^1}$) affording new tetradentate ligands, 2-N-aryl-(2-arylazo)-1,10-phenanthroline ($\mathbf{L^2}$) and tridentate ligands, 4-N-aryl-(2-arylazo)-1,10-phenanthroline ($\mathbf{L^3}$), respectively (Figures 1 and 2; Scheme 3). Among the various nitrogen nucleophiles tested, when primary aromatic amines were used as the nucleophile under the optimized reaction conditions, a significant increase in the yield of the ligand centered aminated product was observed. In absence of substrates(aryl halides), only ligand centered amination was observed. The newly formed ligands $\mathbf{L^2}$ and $\mathbf{L^3}$ obtained using primary aromatic amines as the nucleophiles were isolated from the reaction mixture and identified using X-ray crystallographic analysis. Iron complexes of the newly formed *para*-aminated tridentate azo-aromatic ligand, 4-N-aryl-(2-arylazo)-1,10-phenanthroline ($\mathbf{L^{3b}}$) was also used to study the C–N cross coupling reactions to check the electronic effects of the coordinated ligands on the C–N bond formation reactions (Table 1, entry 18). Several control experiments and DFT calculations were performed to understand the competitive substrate versus ligand centered amination reactions using these Fe-complexes of $\mathbf{L^1}$.

RESULTS AND DISCUSSION

Synthesis and Characterization of Catalysts. The penta-coordinated Fe(II)-catalysts, $[Fe^{II}(L^{1a,b})Cl_2]$ (**1a**, **1b**), were synthesized following a reported literature method using >99.99% $FeCl_2$ obtained from Sigma-Aldrich.[14a] $[Fe^{II}L^{1c}Cl_2]$ (**1c**) was synthesized by stirring dichloromethane solution of the ligand ($\mathbf{L^{1c}}$) in the presence of excess $FeCl_2$ (see Experimental Section for details) (Scheme 2).

The Fe(III)-complexes $[Fe^{III}(L^{1a,b})Cl_2]$ (**2a**, **2b**) were synthesized via the reaction of >99.99% pure $FeCl_3$ and $\mathbf{L^{1a,b}}$

DOI: 10.1021/acs.inorgchem.8b02877
Inorg. Chem. XXXX, XXX, XXX–XXX

Scheme 2. Synthesis of Catalysts 1a, 1b, 1c and 2a, 2b, 2c

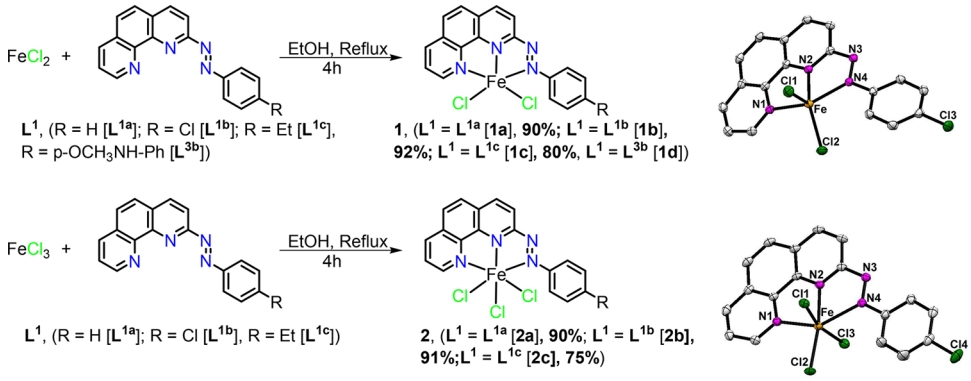

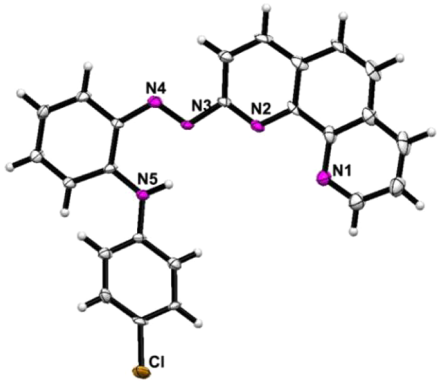

Figure 1. ORTEP representation of L^{2c} with ellipsoids drawn at the 50% probability level. Hydrogen atoms are omitted for clarity (N3–N4: 1.256(3) Å).

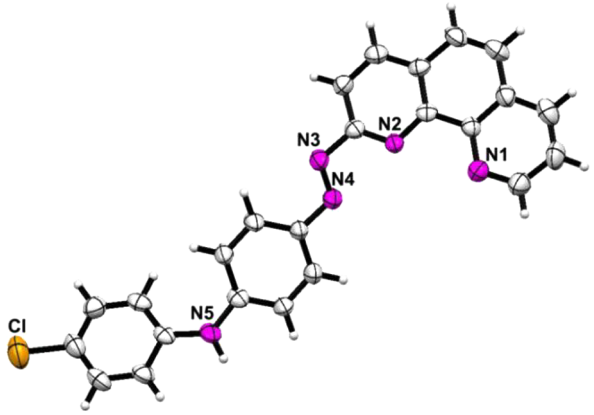

Figure 2. ORTEP representation of L^{3c} with ellipsoids drawn at the 50% probability level. Hydrogen atoms are omitted for clarity (N3–N4: 1.262(4) Å).

in refluxing ethanol. New red colored air stable neutral complexes $[Fe(L^{1a,b})Cl_3]$ (**2a**, **2b**) were obtained in nearly 85% yield (Scheme 2). Elemental analyses of **1c**, **2a**, and **2b** convincingly support their formulations. The identity as well as the electronic structure formulation of **2b** was also affirmed by X-ray single crystal analysis followed by SQUID magnetometry and Mössbauer spectroscopic analysis (see Supporting Information for details). It is worth mentioning here that complexes **2a** and **2b** upon reduction transform to complexes **1a** and **1b**, respectively.

Catalytic C–N Coupling Reactions. In our recent work, we showed that in the presence of 1.0 equiv of KO^{t}Bu, the complex $[Fe^{II}(L^{1b})Cl_2]$ (**1b**) undergoes one electron reduction to produce the monoanionic complex $[Fe^{II}\{(L^{1b})^{\bullet-}\}Cl_2]^-$ ($[\mathbf{1b}]^-$) in 63% yield in 5 h and at 75 °C, 72% conversion of **1b** to $[\mathbf{1b}]^-$ was observed in toluene within 3 h.[14a] Therefore, to begin with, we used the penta-coordinated complexes $[Fe^{II}(L^{1a\text{-}c})Cl_2]$ (**1a–c**) to study the C–N cross coupling reactions between aryl halides and aromatic N-nucleophiles in the presence of KO^{t}Bu as the base. Our intention was to generate the one electron reduced species $[Fe^{II}\{(L^{1a\text{-}c})^{\bullet-}\}Cl_2]^-$($[\mathbf{1a\text{-}c}]^-$) in situ via the KO^{t}Bu mediated reduction of **1a–c** as reported earlier.[14a]

The reaction of 1H-pyrazole (**3a**) and iodobenzene (**4a**) was studied under various reaction conditions to find out the optimal conditions and to explore the solvent and ligand effects on the possibility of catalytic C–N bond formation reactions catalyzed by **1a**. The reaction proceeded most efficiently in DMSO at 120 °C using 10 mol % of the catalyst in the presence of 2.0 equiv of KO^{t}Bu. Lowering the temperature of the reaction led to a significant decrease in yield. Among the different bases examined, the bases like NaOMe, NaOH, K_2CO_3, K_3PO_4, Cs_2CO_3, and DBU, which are known to be nonreducing, were found to be either less effective or ineffective to bring about the desired C–N cross-coupling

Scheme 3. Competitive C–N Bond Formation Reactions

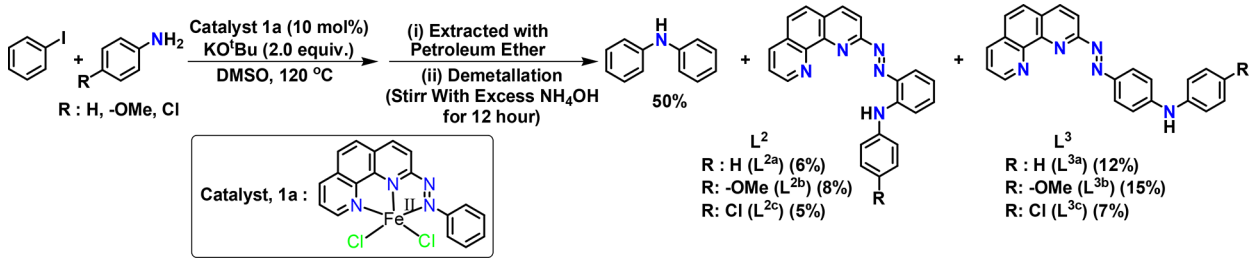

DOI: 10.1021/acs.inorgchem.8b02877
Inorg. Chem. XXXX, XXX, XXX–XXX

Table 1. Optimization of Reaction Conditions[abcd]

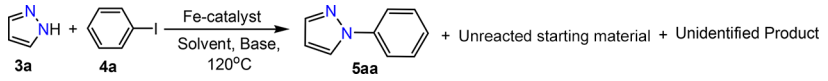

entry	Fe-catalyst (mol %)	solvent	base	time (h)	yield (%)
1	**1a** (10 mol %)	toluene	KO^{t}Bu	36	trace
2	**1a** (10 mol %)	DMF	KO^{t}Bu	36	trace
3	**1a** (10 mol %)	Dioxane	KO^{t}Bu	36	trace
4	**1a** (10 mol %)	THF	KO^{t}Bu	36	trace
5	**1a** (10 mol %)	DMSO	KO^{t}Bu	36	68
6	**1a** (10 mol %)	DMSO	NaH	36	trace
7	**1a** (10 mol %)	DMSO	Cs_2CO_3	36	trace
8	**1a** (10 mol %)	DMSO	K_2CO_3	36	trace
9	**1a** (10 mol %)	DMSO	K_3PO_4	36	trace
10	**1a** (10 mol %)	DMSO	DBU	36	30
11	**1a** (10 mol %)	DMSO	KOH	36	35
12	**1a** (10 mol %)	DMSO	NaOH	36	35
13	**1a** (10 mol %)	DMSO	NaO^{t}Bu	36	67
14	**2a** (10 mol %)	DMSO	KO^{t}Bu	36	65
15	**1b** (10 mol %)	DMSO	KO^{t}Bu	36	57
16	**2b** (10 mol %)	DMSO	KO^{t}Bu	36	53
17	**1c** (10 mol %)	DMSO	KO^{t}Bu	36	68
18	**1d**(10 mol %)	DMSO	KO^{t}Bu	36	70
19	**1a** (7.0 mol %)	DMSO	KO^{t}Bu	36	56
20	[**1a**]$^-$ (8.0 mol %)	DMSO	KO^{t}Bu	36	69
21	[**1a**]$^-$ (8.0 mol %)	DMSO	DBU	36	67
22	[**1a**]$^-$ (8.0 mol %)	DMSO	NaOH	36	69
23	[**1a**]$^-$ (8.0 mol %)	DMSO	KOH	36	67
24	$\mathbf{L}^{1a}$ (10 mol %)	DMSO	KO^{t}Bu	36	
25	$FeCl_2$ (>99.99%)	DMSO	KO^{t}Bu	36	trace
26	$FeCl_3$ (>99.99%)	DMSO	KO^{t}Bu	36	trace
27	$FeCl_2$ (>99.99%) + L (1:1)	DMSO	KO^{t}Bu	36	40
28	$FeCl_3$ (>99.99%) + L (1:1)	DMSO	K^{t}BuO	36	40
29	**1a** + TEMPO	DMSO	K^{t}BuO	36	

[a]Stoichiometry: pyrazole (**3a**) (1.0 mmol; 1.0 equiv) and iodobenzene (**4a**) (1.2 mmol; 1.2 equiv). [b]Under argon atmosphere. [c]Base: 2.0 equiv. [d]Isolated yields after column chromatography.

reactions. The desired C−N coupled products were obtained in high yield with bases like NaO^{t}Bu or KO^{t}Bu. No desired C−N coupled product was obtained in absence of a base. Our repeated attempts on lowering the catalyst loading below 10 mol % decreased the yield significantly. On the other hand, increasing the catalyst loading to 20 mol % did not improve the yield of the C−N coupled product.

[$Fe^{III}L^{1a}Cl_3$] (**2a**), having iron in the +3 oxidation state, also showed a similar type of activity. However, because of the higher price of >99.99% $FeCl_3$ compared to that of >99.99% $FeCl_2$, it was not used for further studies. Interestingly, the Fe-catalysts [$Fe^{II}L^{1b}Cl_2$] (**1b**) and [$Fe^{III}L^{1b}Cl_3$] (**2b**) bearing Cl^- group at the *para*-position of the phenyl ring of the coordinated ligand were found to be less effective in the catalytic C−N cross coupling reactions. On the other hand, introduction of an electron donating ethyl group at the *para*-position of the phenyl ring of the coordinated azo-aromatic ligand does not improve the yield significantly (Table 1, entry 17). Reactions were also performed with the newly synthesized iron-complex, [$FeL^{3b}Cl_2$] (**1d**) containing the *para*-aminated ligand 4-N-(*p*-anisyl)-(2-phenylazo)-1,10-phenanthroline ($\mathbf{L}^{3b}$). To our delight, this complex was also found to be effective in bringing about the desired C−N cross coupling reactions. Slightly higher yields were obtained with the Fe-complexes of 4-N-aryl-(2-arylazo)-1,10-phenanthroline ligands having electron donating -OMe substituent (Table 1, entry 18). However, because of low yield of $\mathbf{L}^{1c}$ and $\mathbf{L}^{3b}$, further studies were performed using [$FeL^{1a}Cl_2$] (**1a**).

To check the role of complex [**1**]$^-$ (formed in situ via KO^{t}Bu mediated reduction) during catalytic C−N coupling reactions, we repeated the coupling of 1H-pyrazole (**3a**) and iodobenzene (**4a**) under the optimized conditions, using the preformed [**1a**]$^-$ as the catalyst. As reported earlier during catalytic dehydrogenation of alcohols,[14a] the catalytic C−N coupling reaction also proceed efficiently using [**1a**]$^-$ as the catalyst, affording the desired 1-phenyl-1H-pyrazole (**5aa**) in 69% yield (Table 1, entry 20). Almost comparable yield of the desired C−N coupled products were obtained with slightly lower catalyst loading. Reactions were also found to proceed with bases such as NaOH, KOH, DBU, which were otherwise found to be less effective when used with the unreduced complex **1a** as the catalyst (Table 1, entries 20−23).

Therefore, all further catalytic reactions were studied using [$Fe^{II}L^{1a}Cl_2$] (**1a**) (10 mol %) as the catalyst, DMSO as the solvent, and KO^{t}Bu as the base. It is important to mention here that DMSO in combination with potassium tertiary butoxide produces dimsyl radical, which may also take part in the catalytic reactions. To check such possibilities, the catalytic reactions were performed in neat conditions (in absence of DMSO as the solvent) with some of the nucleophiles, which

DOI: 10.1021/acs.inorgchem.8b02877
Inorg. Chem. XXXX, XXX, XXX−XXX

Table 2. N-Arylation of 1H-Pyrazole with Various Substituted Aryl Halides[abcdef]

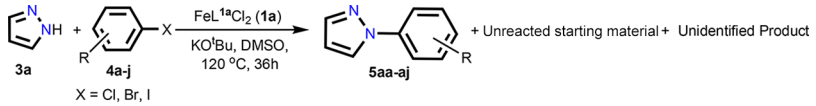

Sl No.	Nucleophile	Iodobenzene	Product	Yield (%)
1		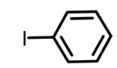	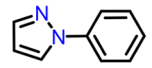 (**5aa**)	68 (65)
2		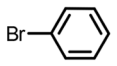	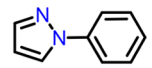 (**5aa**)	40 (35)
3		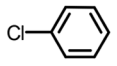	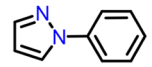 (**5aa**)	NR (NR)
4		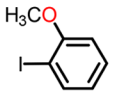	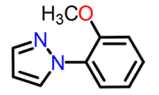 (**5ab**)	65 (64)
5		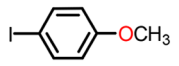	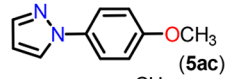 (**5ac**)	71 (65)
6		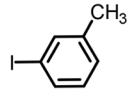	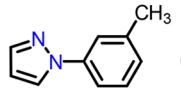 (**5ad**)	57(55)
7		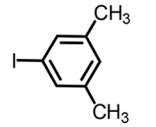	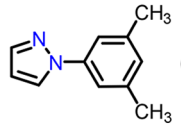 (**5ae**)	45 (43)
8		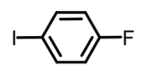	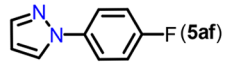 (**5af**)	57 (58)
9		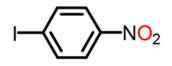	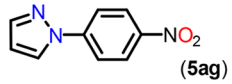 (**5ag**)	60 (58)
10		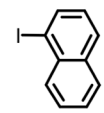	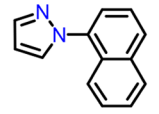 (**5ah**)	61 (60)
11			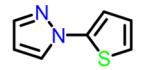 (**5ai**)	40 (36)
12			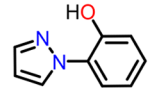 (**5aj**)	68 (69)

[a]Stoichiometry: nucleophile (**3a**) (1.0 mmol; 1.0 equiv) and iodobenzene (**4a-j**) (1.2 mmol; 1.2 equiv). [b]2.0 equiv of KO^{t}Bu. [c]10 mol % catalyst. [d]Under argon atmosphere. [e]Isolated yields after column chromatography. [f]Yields in the parentheses were obtained when preformed [**1a**]$^-$ was used as the catalyst and NaOH as base.

are liquid at room temperature or melts at 130 °C. The reaction was found to proceed smoothly even in absence of any added solvent like DMSO; however, the desired products were obtained in slightly lower yields.

To explore the versatility and the substrate scope of these well-defined Fe-catalysts, a variety of aryl halides (iodo, bromo, chloro) were used to study the catalytic C−N cross coupling reactions under the optimized reaction conditions using 1H-pyrazole (**3a**) as the nucleophilic counterpart. The desired C−N coupled products were obtained in almost comparable yields using either **1a** (10 mol %) and 2.0 equiv. KO^{t}Bu or the monoanionic species [**1a**]$^-$ (8.0 mol %) in combination with NaOH or DBU (1.5 equiv) as the base. The results are summarized in Table 2.

Since aryl iodides are more reactive than aryl bromides, a higher yield of the N−arylated product was obtained using iodobenzene compared to bromobenzene. Using aryl chlorides, only a trace amount of the N-arylated product was isolated. Aryl iodides containing electron donating as well as electron withdrawing functionalities proved to be effective in the catalytic C−N cross coupling reaction with 1H-pyrazole. The desired N-arylated products were obtained in higher yields starting from aryl iodides bearing electron donating groups at the *ortho*- or *para*-positions. For example, reaction of 1H-pyrazole with 4-iodoanisole produced the corresponding N-arylated product in 71% isolated yield (Table 2, entry 5).

Electron-donating groups occupying the *meta*-position of the aryl iodides do not seem to have any effect on the catalytic

DOI: 10.1021/acs.inorgchem.8b02877
Inorg. Chem. XXXX, XXX, XXX−XXX

turnover. Aryl iodides having electron-withdrawing groups were also found to be compatible, although the corresponding N-arylated products were obtained in moderate to low yield (Table 2, entries 8, 9). Reaction with 1-iodonaphthalene as the electrophilic counterpart also produced the corresponding N-arylated product in moderate yield (Table 2, entry 10). The C−N cross-coupling protocol was also found to proceed with heterocyclic iodides, albeit producing the corresponding N-arylated products in lower yield (Table 2, entry 11). The poor yields obtained when using the heterocyclic iodides may be attributed to their coordinating ability, blocking the Fe-center of the catalyst. This methodology was found to be selective, as the reaction of 2-iodo phenol with 1H-pyrazole produced the corresponding N-arylated product, and no C−O bond formation was observed (Table 2, entry 12).

To further expand the substrate scope, several reactions employing a diverse range of N-nucleophiles including 1H-imidazole, 1H-indole, benzimidazole, triazole, morpholine, pyrrole, benzamide, etc. were carried out under the optimized reaction conditions with iodobenzene using **1a** as the catalyst and KO^{t}Bu as the base. With all these nucleophiles, the corresponding N-arylated products were isolated in moderate to good yields. For example, 1H-imidazole, when reacted with iodobenzene under the optimized reaction conditions, produced 1-phenyl-1H-imidazole (**5ba**) in 72% isolated yield (Table 3, entry 2). Reaction of 1H-indole with iodobenzene under the optimized reaction conditions afforded 1-phenyl-1H-indole (**5ca**) in 60% isolated yield (Table 3, entry 3). 1-Phenyl-1H-benzo[d]imidazole (**5da**) was obtained in 61% isolated yield form the reaction of 1H-benzo[d]imidazole and iodobenzene under the optimized reaction conditions (Table 3, entry 4). Reactions of iodobenzene with piperidine, pyrrolidine, and morpholine produced the desired C−N coupled products in 69, 73, and 72% isolated yields, respectively (Table 3, entries 7−9). Triazoles were also found to be effective; however, the yields of the desired C−N coupled products are comparatively low (Table 3, entries 10, 11). Amides were also found to be compatible, the reaction of benzamide with iodobenzene also afforded the corresponding *N*-phenylbenzamide in 42% isolated yield (Table 3, entry 12), whereas the cyclic amide derivative (pyrrolidin-2-one) produced the corresponding N-arylated product in 50% yield (Table 3, entry 13).

Primary amines were also found to be effective for the C−N cross coupling reactions, catalyzed by **1a**. Reaction of aniline with iodobenzene produced diphenylamine (**5na**) in 50% isolated yield (Table 3, entry 14). N-Arylation of iodobenzene was even achieved with cyclohexylamine; N-cyclohexylaniline (**5oa**) was obtained in 45% isolated yield (Table 3, entry 14). It is worthy to mention that while varying different nucleophiles, we tried to understand the reactivity pattern, whether it follows any order depending on the pK_a of the attached proton. However, experimental results obtained in our case as well as with other already reported copper catalyzed reactions do not show such type of straightforward correlation with the pK_a of the attached proton and hence it seems to be a overall combined effect.[6,7]

It is noteworthy to mention here that, during chromatographic purification of the reaction mixtures of iodobenzene and aniline as the nucleophile, we first observed a blue colored complex in the column. Our attempts to isolate the blue colored complex from the catalytic reaction mixture was not successful. Even after scaling up the catalytic reaction and

Table 3. N-Arylation of Nitrogen Nucleophiles with Iodobenzene Catalyzed by [Fe(L^{1a})Cl$_2$] (1a)[abcde]

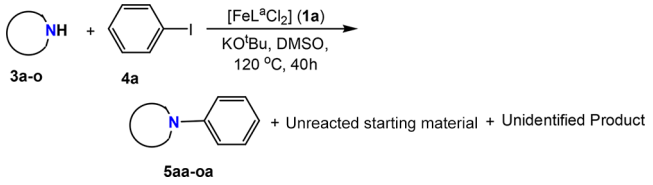

Sl No.	Nucleophile	Iodobenzene	Product	Yield (%)
1			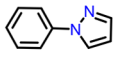	(5aa) 67
2			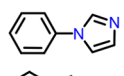	(5ba) 72
3			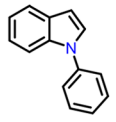	(5ca) 60
4			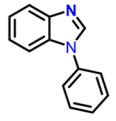	(5da) 61
5	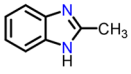		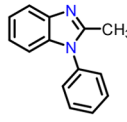	(5ea) 51
6	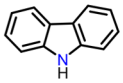		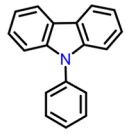	(5fa) 55
7			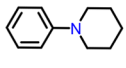	(5ga) 69
8			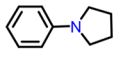	(5ha) 73
9			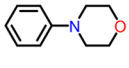	(5ia) 72
10			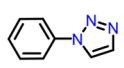	(5ja) 41
11			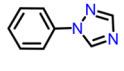	(5ka) 45
12	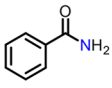		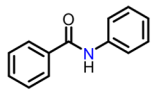	(5la) 42
13			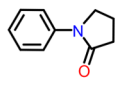	(5ma) 50
14				(5na) 50
15				(5oa) 45

[a]Stoichiometry: nucleophile (**3a**-o) (1.0 mmol; 1.0 equiv) and iodobenzene (**4a**) (1.2 mmol; 1.2 equiv). [b]2.0 equiv of KO^{t}Bu. [c]10 mol % catalyst. [d]Under argon atmosphere. [e]Isolated yields after column chromatography.

DOI: 10.1021/acs.inorgchem.8b02877
Inorg. Chem. XXXX, XXX, XXX−XXX

Scheme 4. Ligand Centered C−N Coupling in Absence of Substrate (Iodobenzene)

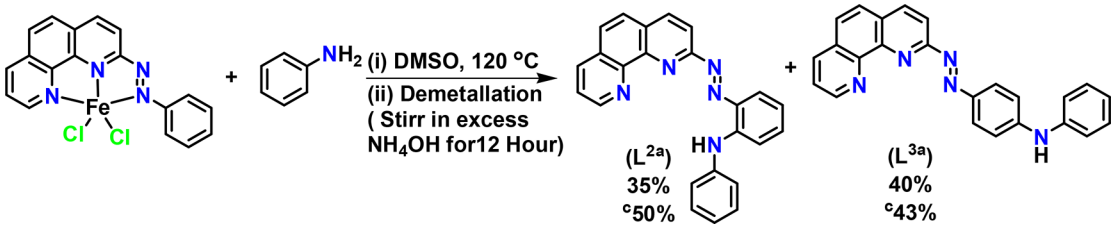

[c]Neat conditions.

increasing the catalyst loading to 25 mol %, we could not manage to isolate the blue colored complex from the catalytic reaction mixture. Literature survey showed that similar blue-colored complex formation was observed by Goswami and co-workers when they reacted transition-complexes of 2-arylazopyridine ligands with primary aromatic amines.[15,16] In their study, they reported metal mediated C−N bond formation at the *ortho*- and *para*-positions of the coordinated 2-arylazopyridine ligands and the observed blue color was proposed to originate from the uncoordinated -NHPh to π^* (azo) transition.

To check the possibility of such type of C−N bond formation at the phenyl ring of the coordinated 2-(phenylazo)-1,10-phenanthroline ligand ($\mathbf{L^{1a}}$), demetalation reaction was carried out to isolate the pure organic ligand (Scheme 3). In a typical reaction, the ethanol solution of the blue colored complex was stirred overnight in the presence of excess ammonium hydroxide, which leads to demetalation and formation of iron hydroxide salts. After filtration of this reaction mixture and usual workup, the organic part was purified by column chromatography, which indeed allowed us to isolate two new red colored organic ligands $\mathbf{L^{2a}}$ and $\mathbf{L^{3a}}$, respectively, of same molecular mass of 376 amu having an extra PhNH-moiety attached to the parent ligand $\mathbf{L^{1a}}$. The simulated isotropic distribution of these two mass spectra matches well with the given same formula (see Supporting Information). To check the generality of these ligand centered amination reactions, 4-methoxy aniline and 4-chloro aniline were used as the nucleophiles, and after similar demetalation we successfully isolated $\mathbf{L^{2b,c}}$ and $\mathbf{L^{3b,c}}$ from the reaction mixtures. ^{1}H NMR spectra of $\mathbf{L^{2a}}$ and $\mathbf{L^{3a}}$ indeed confirm the formation of two new organic ligands containing an additional −NHPh arm when compared to parent ligand $\mathbf{L^{1a}}$ (see Supporting Information). Further characterization by single crystal X-ray diffraction certainly approves the formation of C−N bond at the *ortho*- and *para*-positions of $\mathbf{L^{1a}}$ (see further).

X-ray quality single crystals of the ligand $\mathbf{L^{2c}}$ were grown via slow evaporation of its dichloromethane/hexane (10:1) solution. An ORTEP representation of $\mathbf{L^{2c}}$ is displayed in Figure 1. Formation of a new tetradentate scaffold 2-[(2-*N*-phenylamino)phenylazo]-1,10-phenanthroline ($\mathbf{L^{2c}}$) via the construction of a new C−N bond at the *ortho*-position of the parent azo-aromatic ligand $\mathbf{L^{1a}}$ is indeed confirmed from the single crystal structure of $\mathbf{L^{2c}}$. The N=N distance was found to be 1.256(3) Å.

Similarly, single crystals of the ligand $\mathbf{L^{3c}}$ were grown via slow evaporation of its dichloromethane/hexane (10:1) solution. ORTEP representation of $\mathbf{L^{3c}}$ is shown in Figure 2. The formation of a new C−N bond at the *para*- position of the azo-aromatic ligand $\mathbf{L^{1a}}$ affording a new tridentate azo-aromatic ligand 2-[(4-*N*-phenylamino)phenylazo]-1,10-phenanthroline ($\mathbf{L^{3c}}$) is indeed confirmed from the X-ray structure. The N=N distance was found to be 1.262(4) Å.

These results using primary aromatic amines as the nucleophiles indeed show competitive substrate(iodobenzene) versus ligand centered C−N bond formation reactions. Control reactions in absence of substrate (iodobenzene) only showed ligand centered amination reaction (Scheme 3). However, in absence of metal ion, when the free ligands were subjected for C−N cross-coupling reaction under the optimized reaction conditions, no ligand centered amination was observed. It is worthy to mention here that in similar complexes *ortho*- C−N bond formation is observed only when there is some vacant coordination site or labile ligands are available at the metal center. For stable, coordinatively saturated and kinetically inert transition metal complexes where there is no such vacant coordination site available, only *para*-amination reactions were observed.[16] Therefore, The C−N bond formation reaction at the *ortho*-position of the coordinated ligand $\mathbf{L^1}$ is believed to proceed via an inner sphere mechanism where the coordination of the nucleophile to the iron-center is one of the steps for the reaction to proceed. On the other hand, the C−N bond formation at the *para*-position of the coordinated ligand $\mathbf{L^1}$ is believed to be an outer-sphere nucleophilic substitution. In line with our arguments, in absence of the competitor substrate-(iodobenzene), the ligand centered C−N bond formation both at the *ortho*- and *para*-positions was found to increase substantially (Scheme 4).

Ligand centered amination using primary aromatic amine and isolation of two new series of azo-aromatic ligands $\mathbf{L^{2a-c}}$ and $\mathbf{L^{3a-c}}$ prompted us to recheck the reaction mixtures of various nitrogen nucleophiles and iodobenzene. ESI-MS spectra of the catalytic C−N coupling reactions between 1H-pyrazole with iodobenzene also point to a competitive substrate(aryl halides) versus ligand centered amination reactions (see Supporting Information).

Control Experiments and DFT Studies To Obtain Mechanistic Insight into Observed Competitive Substrate versus Ligand Centered C−N Coupling. To understand the mechanism, some control experiments were carried out. In absence of the catalyst [$FeL^{1a}Cl_2$] (**1a**), no desired C−N coupled product was obtained. Using >99.99% $FeCl_2$ or >99.99% $FeCl_3$, obtained from Aldrich, only a trace amount of the N-arylated product was obtained as reported earlier by Buchwald and Bolm.[6i] The lower reactivity may be attributed to the thermodynamically unfavorable metal centered redox events associated with the different elementary steps of the C−N cross coupling reactions; however, the exact reason of low reactivity of pure iron salts is not completely understood. Moreover, instead of using the preformed catalyst

DOI: 10.1021/acs.inorgchem.8b02877
Inorg. Chem. XXXX, XXX, XXX−XXX

$[FeL^{1a}Cl_2]$ (**1a**), when a 1:1 mixture of >99.99% $FeCl_2$ or >99.99% $FeCl_3$ (obtained from Aldrich) and L^{1a} was used, a significant decrease of product yield was observed (Table 1, entry 27, 28). To rule out the possibility of contaminants,[6i−l] all the catalytic reactions were performed using properly washed single crystals of the iron complex. To check the possibility of any copper or palladium contamination present in our catalyst samples, inductively coupled plasma mass spectrometry (ICPMS) experiments were carried out. Presence of only 37 ppb of copper and 02 ppb of palladium impurities have been detected, which are far below the level (5.0 ppm) of copper impurities known to produce 97% of C−N coupled product in the presence of DMEDA ligand.[6i] To check other possible sources of copper and palladium, KO^{t}Bu and DMSO have also been analyzed using ICPMS. However, no copper or palladium impurities have been detected. Next to be more sure about the possibility of contaminations in/on the glassware that we used during the catalytic reactions, 1H-pyrazole and iodobenzene were refluxed in DMSO at 130 °C in randomly selected Schlenk tubes available in our laboratory. Four different Schlenk tubes were used for these control reactions and in all the cases no C−N coupled product was obtained. As a further control experiment, the cross-coupling of 1H-pyrazole (**3a**) and iodobenzene (**4a**) was carried out under optimized reaction conditions using a similar copper(II) complex, CuL^1Cl_2, synthesized via the reaction of L^1 with $CuCl_2$ under the similar reaction conditions reported for $[FeL^1Cl_2]$.[14a] After repeated experiments using CuL^1Cl_2 (1.0 ppm) as catalyst, we obtained only 7−10% of the desired C−N coupled product. The results obtained from these above experiments confirm the definite involvement of our catalyst, $[FeL^{1a}Cl_2]$ (**1a**), in the catalytic turnover.

The coordinated ligand is redox noninnocent and undergoes reduction to produce an azo-anion radical. Therefore, to probe the formation of any organic radical as well as to confirm the participation of the coordinated ligand during catalysis, a radical scavenger was used while carrying out the catalytic reactions. In presence of one equivalent of TEMPO, the catalytic reaction was totally shut down. It is noteworthy to mention here that, in the presence of excess KO^{t}Bu, the complexes $[Fe(L^{1a/b})Cl_2]$ (**1a/b**) undergo one-electron reduction producing azo-anion radical complexes $[Fe^{II}\{(L^{a/b})^{\bullet-}\}Cl_2]^-$ ($[\mathbf{1a/b}]^-$), which then act as the actual catalyst in C−N coupling reactions as was reported previously during catalytic dehydrogenation of benzylic alcohols.[14a] Indeed, the prereduced catalyst $[\mathbf{1a}]^-$ showed almost similar type of efficiency during C−N cross-coupling reactions as was observed during optimizations (see Table 1 and 2).

On the basis of available literature and the conclusions drawn from various control experiments mentioned above, a plausible mechanism is outlined in Scheme 5. The reaction is believed to begin with the KO^{t}Bu-mediated reduction of **1** to form the active catalyst azo-anion radical complex **A** ($[\mathbf{1}]^-$), which then undergoes oxidative addition with iodobenzene to produce the intermediate **B**. This two-electron step is believed to involve concerted one-electron oxidation of both the metal and the ligand radical, to produce intermediate **B**. In the next step, the deprotonated nucleophile binds the Fe-center to form the intermediate **C**. Finally, intermediate (**C**) undergoes reductive elimination to release the desired product.

DFT calculations were performed to further explore the mechanism of the present iron-catalyzed C−N cross coupling reactions (for details, see Experimental Section and Supporting Information). Plausible low-barrier C−N coupling pathways were investigated at the BP86 and def2-TZVP level using $[\mathbf{1a}]^-$ as the catalyst (Scheme 6). Activation of the Ar−I bond is the first step in the computed catalytic cycle. Neutral complex **B′** is formed upon displacement of Cl^- in anionic complex **A**. It is difficult to calculate thermodynamic energy differences for displacement reactions where the charge is not constant. Under the reaction conditions, however, such transformations are easily accessible. Cleavage of the Ar−I bond in **B′** leads to formation of **B** via **TS-1** with a barrier of +16.7 kcal mol^{-1}. We also considered coordination of Ar in a different fashion with the aryl group directed away from the 2-(arylazo)-1,10-phenanthroline ligand. This pathway proceeds with a relatively higher barrier of +21.2 kcal mol $^{-1}$ and leads to $\mathbf{B}_1$, which is an isomer of **B** with the aryl group in the equatorial plane (more details in the Supporting Information).

The next step is the displacement of the iodide ligand in **B** by a deprotonated pyrazole moiety, which leads to the formation of complex **C**. In complex **C**, the noncoordinated N in pyrazole makes a nucleophilic attack on the aryl moiety leading to formation of Ar-Nu adduct **D′** (Scheme 7). The computed barrier for this step is +16.6 kcal mol^{-1}.[17] Other

Scheme 5. Proposed Mechanism

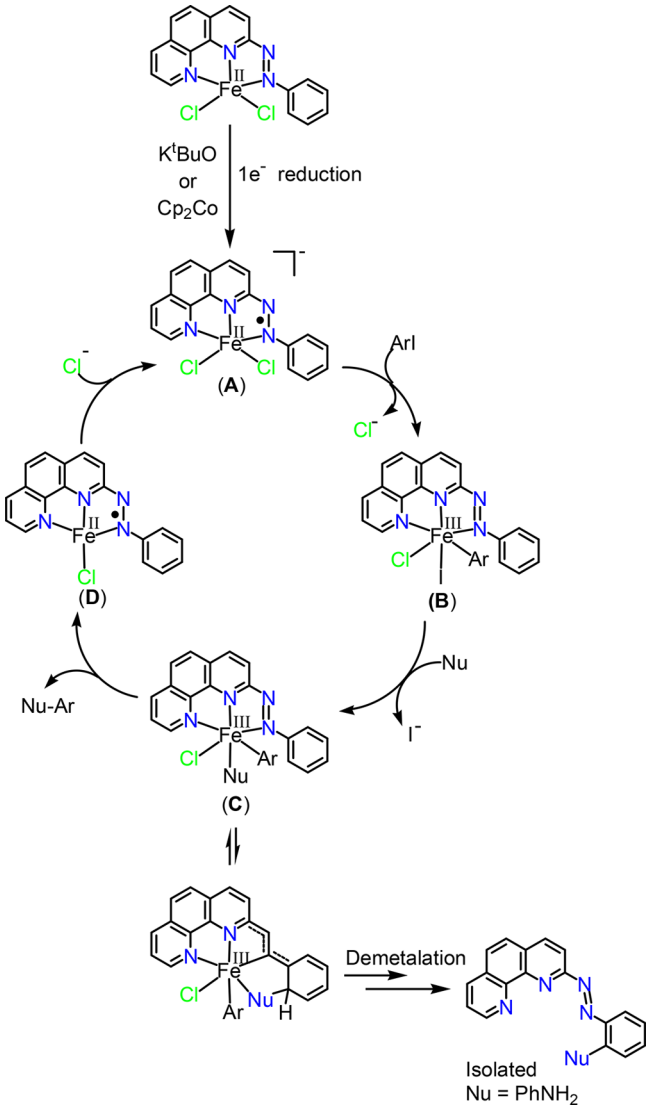

DOI: 10.1021/acs.inorgchem.8b02877
Inorg. Chem. XXXX, XXX, XXX−XXX

Scheme 6. Computed Pathway for Substrate Activation by Cleavage of Aryl−Iodide Bond in Ar−I

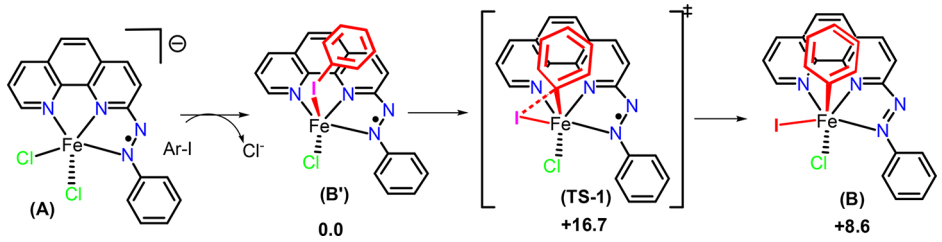

Scheme 7. Computed Pathway for Ar−Nu Coupling after Ar−I Bond Activation

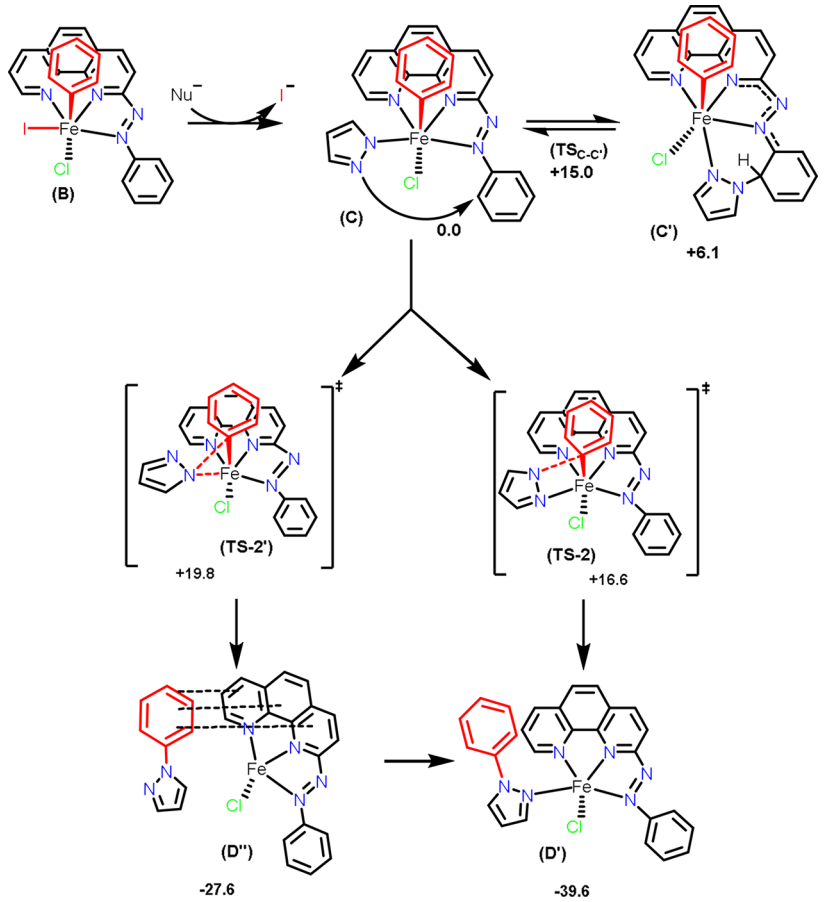

possible pathways for Ar−Nu coupling involving (i) direct nucleophilic attack of another pyrazole N, which is coordinated to Fe, and (ii) Ar−Nu coupling with Ar in axial position were found to proceed with higher barriers (see Supporting Information).[18]

The noncoordinated N in pyrazole in complex **C** can also attack the *ortho*-carbon of the phenyl group of the coordinated ligand, leading to formation of complex **C′** via $\mathbf{TS}_{C-C'}$ over a TS barrier of +15.0 kcal mol^{-1}. Formation of complex **C′** is an endergonic process and it can easily convert back to complex **C** via the backward reaction over a TS barrier of +8.9 kcal mol^{-1}. It is therefore expected that complexes **C** and **C′** are in equilibrium with each other, in agreement with experimental observations (vide supra).

Finally, the direct release of the product from **D′** to form **D** was found to be unfavorable (endergonic by ∼20 kcal mol^{-1}). Instead of a direct release, a Cl^- ligand could add on **D′** to form $\mathbf{A}_{Nu\text{-}Ar}$. The release of Ar−Nu from $\mathbf{A}_{Nu\text{-}Ar}$ to regenerate catalysts **A** was computed to be downhill by 5.3 kcal mol^{-1} with a very small transition state barrier of +1.4 kcal mol^{-1} with respect to the **Ar-Nu** adduct $\mathbf{A}_{Ar\text{-}Nu}$ (Scheme 8).

CONCLUSIONS

In summary, we have reported an alternative approach of iron catalyzed carbon−nitrogen cross coupling reactions of a wide range of nucleophiles and aryl halides using well-defined iron-complexes featuring redox noninnocent 2-(arylazo)-1,10-phenanthroline ligands. In addition to substrate centered C−N coupling, competing C−N coupling reactions were also observed at the *ortho*- and *para*-positions of the phenyl ring of the coordinated azo-aromatic ligands affording new tetradentate ligands, 2-N-aryl-(2-arylazo)-1,10-phenanthroline ($\mathbf{L}^2$) and tridentate ligands, 4-N-aryl-(2-arylazo)-1,10-phenanthroline ($\mathbf{L}^3$), respectively. Mechanistic studies reveal that the active catalyst is the one electron reduced species $[\mathbf{1}]^-$, and both metal and the coordinated ligand participate in a cooperative manner during electron transfer processes involved in the elementary steps of the catalytic reaction. Experimental

DOI: 10.1021/acs.inorgchem.8b02877
Inorg. Chem. XXXX, XXX, XXX−XXX

Scheme 8. Release of Ar−Nu and Catalyst Regeneration

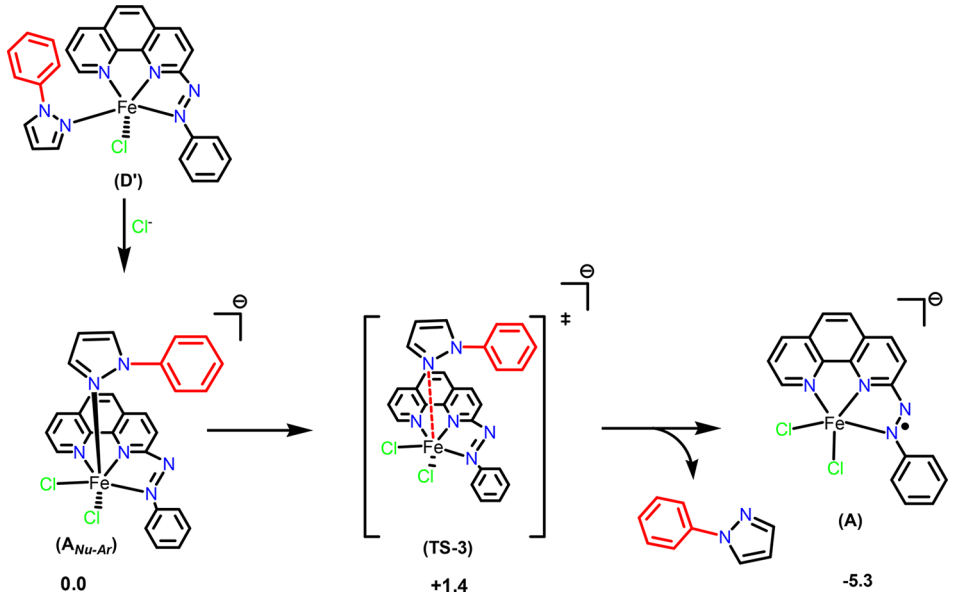

and DFT studies were carried out to understand the competitive substrate versus ligand centered amination reactions. Overall, these results reveal a new window where azo-aromatic ligands in combination with other metal ions can be used to explore various catalytic reactions.

EXPERIMENTAL SECTION

Materials. The >99.99% $FeCl_2$, > 99.99% $FeCl_3$, and iodobenzenes were obtained from Sigma-Aldrich. $L^{1a\text{-}c}$ and $[Fe^{II}L^{1a\text{-}c}Cl_2]$ (**1a−c**) were synthesized following the reported literature methods using >99.99% $FeCl_2$ obtained from Sigma-Aldrich as the iron source.[14] All other starting materials, chemicals, and reagents were obtained from the available commercial sources and used as received.

Physical Measurements. Bruker Avance 300/400/500 MHz and JEOL 400 MHz spectrometers were used for recording ^{1}H NMR spectra. TMS was used as the internal standard. Micro mass Q-TOF mass spectrometer (serial no. YA 263) was used for recording ESI mass spectra. Room temperature magnetic moment measurements for **2b** were carried out with Gouy balance (Sherwood Scientific, Cambridge, U.K.). The Mössbauer spectrum of **2b** was recorded with a ^{57}Co source in a Rh matrix using an alternating constant acceleration *Wissel* Mössbauer spectrometer operated in the transmission mode and equipped with a *Janis* closed-cycle helium cryostat. Isomer shifts are given relative to iron metal at ambient temperature. Using *Quantum-Design* MPMS-XL-5 SQUID magnetometer equipped with a 5 T magnet, variable temperature magnetic moment measurement for **2b** was performed in the temperature range from 295 to 2.0 K at 0.5 T magnetic field. The powdered sample was contained in a gel bucket and fixed in a nonmagnetic sample holder. Each raw data file for the measured magnetic moment was corrected for the diamagnetic contribution of the sample holder and the gel bucket. The molar susceptibility data were corrected for the diamagnetic contribution. An inductively coupled plasma orthogonal acceleration time-of-flight mass spectrometer (ICP-oa-TOF-MS), model: 8000R (GBC, Australia), was used for the determination of copper and palladium impurities. ICPOES (model ULTIMA 2 (Jobin Yvon—Horiba, France) was used to quantify the amount of iron present in the catalyst.

Synthesis. *Synthesis of L^{1c}.* L^{1c} was prepared following the literature procedure[14a] using 2-amino-1,10-phenanthroline and 4-ethylnitrosobenzene as the coupling partners. Yield: 30%. Anal. calcd: C, 76.90; H, 5.16; N, 17.94; found: C, 76.98; H, 5.30; N, 17.87. UV−vis: $\lambda_{max/nm}$ (ε, M^{-1} cm^{-1}), 236 (32,229), 275 (23,501), 350 (25,600). IR (KBr, cm^{-1}): 1701 (ν, C=N), 1418 (ν, N=N). ESI-MS: m/z 313.14 $[L^{1c} + H]^+$. ^{1}H NMR (500 MHz, $CDCl_3$): δ 9.13 (s, 1H), 8.184−8.209 (m, 1H), 8.092−8.077 (t, J = 4 Hz, 1H), 8.03 (d, J = 8 Hz, 2H), 7.99−7.93 (m, 1H), 7.63 (d, 2H), 7.51−7.49 (m, 1H), 7.29 (d, J = 8 Hz, 2H), 2.67−2.62 (m, 2H), 1.19 (t, J = 6 Hz, 3H). ^{13}C NMR (100 MHz, $CDCl_3$): δ162.1, 150.9, 150.5, 149.4, 146.3, 145.6, 138.4, 136.0, 129.4, 129.0, 128.6, 127.5, 126.0, 124.1, 123.2, 113.4, 28.9, 15.2.

*Synthesis of $[FeL^{1a}Cl_2]$ (**1a**) and $[FeL^{1b}Cl_2]$ (**1b**).* Complexes **1a** and **1b** were synthesized following the literature procedure.[14a]

*Synthesis of $[FeL^{1c}Cl_2]$ (**1c**).* One-hundred milligrams (0.320 mmol) of ligand L^c was dissolved in 20 mL of dichloromethane and was taken in a dropping funnel and was added dropwise to a suspension of $FeCl_2$ (127 mg (1.0 mmol)) in dichloromethane in a 100 mL round-bottom flask fitted with a stir bar. The dropwise addition of L^c was continued over 20 min. During this time, the color of the solution in the round-bottom flask changed from light yellow to dark brown. After the addition was complete, the whole solution was stirred for additional 30 min. The solution was then passed through a cotton filter, and the filtrate, thus obtained, was dried under vacuum to obtain a solid residue. Fractional crystallization of the solid residue in dichloromethane/hexane solvent mixture afforded the pure complex **1c**. Yield: 90%. Anal. calcd: C, 54.70; H, 3.67; N, 12.76; found: C, 54.60; H, 3.77; N, 12.67. ESI-MS $[M - Cl^-]^+$: m/z 402.98. UV−vis: $\lambda_{max/nm}$ (ε, M^{-1} cm^{-1}), 239 (17,929), 266 (12,718), 355 (16,829). IR (KBr, cm^{-1}): 1744 (ν, C=N), 1438(ν, N=N).

*Synthesis of $[FeL^{3b}Cl_2]$ (**1d**).* Fifty milligrams (0.123 mmol) of ligand L^{3b} was dissolved in 15 mL of dichloromethane and taken in a dropping funnel and was added dropwise to a suspension of $FeCl_2$ (24.5 mg, 0.193 mmol) in dichloromethane in a 100 mL round-bottom flask fitted with a stir bar. The dropwise addition of L^{3b} was continued for 20 min. During this time, the color of the solution in the round-bottom flask changed from light yellow to dark blue. The whole solution was stirred for additional 30 min and filtered. The filtrate was then evaporated to dryness and fractional crystallization of the solid residue in dichloromethane/hexane solvent mixture yielded the pure complex **1d**. Yield: 80%. Anal. calcd: C, 56.42; H, 3.60; N, 13.16; found: C, 56.32; H, 3.72; N, 13.06. UV−vis: $\lambda_{max/nm}$ (ε, M^{-1} cm^{-1}), 235 (12,609), 292 (9,057), 358 (4,783), 563 (b,555), 767 (b, 1231). IR (KBr, cm^{-1})): 1724 (ν, C=N), 1431(ν, N=N).

*Synthesis of $[FeL^{1a}Cl_3]$ (**2a**).* In ethanol, 50 mg (0.17 mmol) of the ligand (L^{1a}) was allowed to dissolve, and then 27.5 mg (0.17 mmol) of $FeCl_3$ was poured to it. Upon addition of $FeCl_3$, the orange color of the solution instantaneously changed to red, and a dark red colored precipitate appeared after few minutes. The mixture was refluxed for

DOI: 10.1021/acs.inorgchem.8b02877
Inorg. Chem. XXXX, XXX, XXX−XXX

four hours, and the precipitate was then filtered off. The complex was purified by fractional crystallization from dichloromethane/hexane solvent mixtures. Yield: 90%. Anal. calcd: C, 48.42; H, 2.71; N, 12.55; found: C, 48.47; H, 2.80; N, 12.48. UV−vis: $\lambda_{max/nm}$ (ε, M^{-1} cm^{-1}), 231 (16,072), 337 (7,308), 400 (9598). IR (KBr, cm−1): 1705 (ν, C=N), 1450 (ν, N=N).

Synthesis of [FeL^{1b}Cl$_3$] (2b). The complex **2b** was synthesized following the same procedure described for the synthesis of complex **2a**. Yield: 91%. Anal. calcd: C, 44.95; H, 2.31; N, 11.65; found: C, 44.89; H, 2.40; N, 11.73. UV−vis: $\lambda_{max/nm}$ (ε, M^{-1} cm^{-1}), 245 (17,322), 403 (10,231). IR (KBr, cm^{-1}): 1715 (ν, C=N), 1493 (ν, N=N). SQUID Magnetometry: (300−50 K) $\chi_M T$ = 4.37 cm^3 mol^{-1} K. Mossbauer Spectroscopy: δ = 0.48 mm s^{-1}, ΔE_Q = 1.25 mm$_\bullet$ s^{-1}.

General Procedure for Catalytic C−N Bond Formation. In a 50 mL oven-dried Schlenk tube, 1.0 mmol nucleophile, 10.0 mol % catalyst, and 2.0 equiv KO^{t}Bu were added. The tube was capped with a rubber septum. It was then evacuated and argon was backfilled. The same procedure was repeated three times. To this mixture, 1.2 mmol aryl halide, 4.0 mL of dry and degassed DMSO was added using a syringe. All joints were sealed with Teflon tape. The tube was then placed in an oil bath preheated at 120 °C. The reaction was continued for 36 h. Once the reaction was complete, the reaction mixture was cooled to room temperature. The reaction mixture was poured into saturated brine solution (approximately 100 mL). It was then extracted three times with dichloromethane. The combined organic portion was evaporated and subjected to column chromatography using petroleum ether/ethyl acetate as the eluent.

Demetalation and Isolation of L^2 and L^3 from the Catalytic Reaction Mixture. The blue portion, obtained from the reaction mixture during column chromatography, was dissolved in EtOH, and excess NH_4OH was then added to it. Upon addition of NH_4OH, the color of the solution immediately changed from blue to red. The resulting solution was stirred overnight at room temperature. The ethanol was evaporated, and the residue was dissolved in dichloromethane and purified by preparative TLC using ethyl acetate/petroleum ether as the eluent.

Reaction of Complex 1a with Primary Amines in Neat Condition. A 50 mL round-bottom flask was charged with 1.0 mmol of complex **1a**, 2.0 equiv KO^{t}Bu, and excess of aniline (or substituted anilines). The flask was then placed in a water bath and heated for 30 min. During this period, the color of the reaction mixture gradually changed to blue. The excess aniline was removed by repeated washing with hot hexane solution. The blue semisolid compound was then dissolved in EtOH, and excess of NH_4OH was added to it. The solution was stirred overnight. During this period, a black precipitate was formed. The red colored solution, thus obtained, was filtered and dried in vacuum. The residue was purified by preparative TLC to isolate **L$^{2a\text{-}c}$** and **L$^{3a\text{-}c}$** (see Supporting Information for details).

ICPMS and ICPOES Experiments. A 0.0108 g of sample was slowly heated to dryness with 5.0 mL of concentrated nitric acid in a hot plate. This step was repeated twice. After cooling, 2.0% nitric acid was again added into the samples, and the whole content was transferred into a 50 mL volumetric flask with repeated washing of the digestion vessel, and volume was made up with same nitric acid. This 50 mL yellow colored solution was used for estimation of Pd and Cu using ICPMS.

X-ray Crystallography. Suitable X-ray-quality crystals of **2b**, **L^{2c}**, and **L^{3c}** were grown via slow evaporation of their dichloromethane−hexane (10:1) solutions. The X-ray data of **2b**, **L^{2c}**, and **L^{3c}** were collected on a Bruker SMART Apex II diffractometer equipped with a CCD area detector, with monochromated Mo Kα radiation (λ = 0.71073 Å). **2b**: Out of the total 29134 reflections collected, 5066 unique (R_{int} = 0.024) reflections satisfying the ($I > 2\sigma(I)$) criterion were used for the final X-ray structure analysis. **L^{2c}**: Out of the total 46 137 reflections collected, 7405 unique (R_{int} = 0.127) reflections satisfying the ($I > 2\sigma(I)$) criterion were used for the final X-ray structure analysis. In the single-crystal structure of **L^{2c}**, the hydrogen atoms bonded to O200 of water solvent molecule were not discernible from the last final difference Fourier map, and consequently their positions were not considered. **L^{3c}**: Out of the total 30 924 reflections collected, 7160 unique (R_{int} = 0.216) reflections satisfying the ($I > 2\sigma(I)$) criterion were used for the final X-ray structure analysis.

SAINT-NT software package was used for data reduction.[19] Using SADABS program, multiscan absorption correction was applied to all intensity data.[20] Combination of direct methods followed by difference Fourier syntheses were used to solve the structures. Full-matrix least-squares refinement was done on F2 using the SHELX-2013 program.[21] Anisotropic thermal displacements were employed during refinement of all non-hydrogen atoms. The details of the X-ray crystal structures along with the refinement details are summarized in Table S1.

Computational Details. All DFT geometry optimizations were performed with the Turbomole program[22] coupled to the PQS Baker optimizer[23] via the BOpt package.[24] Geometries were fully optimized as minima or transition states using the BP86 functional[25] and the resolution-of-identity (ri) method[26] using the Turbomole def2-TZVP basis[27] for all atoms. Grimme's dispersion corrections (D3 version, implemented with the keyword disp3 in Turbomole) were applied in all geometry optimizations.[28] All minima (no imaginary frequencies) and transition states (one imaginary frequency) were characterized by calculating the Hessian matrix. ZPE and gas-phase thermal corrections (entropy and enthalpy, 298 K, 1 bar) from these analyses were calculated. The relative (free) energies obtained from these calculations are reported in the main text of this paper. Intrinsic reaction coordinate (IRC) calculations were performed to confirm the nature of the transition states.

By calculation of the partition function of the molecules in the gas phase, the entropy of dissociation or coordination for reactions in solution was overestimated (overestimated translational entropy terms in the gas phase compared to solutions). For reactions in solution, we therefore corrected the Gibbs free energies for all steps involving a change in the number of solute species. The applied correction term is a correction for the condensed phase (CP) reference volume (1 L mol^{-1}) compared to the gas phase (GP) reference volume (24.5 L mol^{-1}). This leads to an entropy correction term ($S_{CP} = S_{GP} + R \ln\{1/24.5\}$) for all species, which, combined with neglecting the RT term, corrects the relative free energies (298 K) of all associative (−2.5 kcal mol^{-1}) and dissociative steps (+2.5 kcal mol^{-1}).[29]

■ ASSOCIATED CONTENT

Supporting Information

The Supporting Information is available free of charge on the ACS Publications website at DOI: 10.1021/acs.inorgchem.8b02877.

ESI-MS spectra, ^{1}H NMR spectra, ORTEP, Cartesian coordinates of optimized structures (PDF)

Accession Codes

CCDC 1847828−1847830 contain the supplementary crystallographic data for this paper. These data can be obtained free of charge via www.ccdc.cam.ac.uk/data_request/cif, or by e-mailing data_request@ccdc.cam.ac.uk, or by contacting The Cambridge Crystallographic Data Centre, 12 Union Road, Cambridge CB2 1EZ, UK; fax: +44 1223 336033.

■ AUTHOR INFORMATION

Corresponding Author

*E-mail: ndpaul@gmail.com.

ORCID

Vivek Sinha: 0000-0002-6856-9469

Franc Meyer: 0000-0002-8613-7862

Nanda D. Paul: 0000-0002-8872-1413

Author Contributions

#S.S. and R.S. contributed equally to this work.

DOI: 10.1021/acs.inorgchem.8b02877
Inorg. Chem. XXXX, XXX, XXX−XXX

Author Contributions

[¶]V.S. performed the computational work.

Notes

The authors declare no competing financial interest.
U.J. died on August 31, 2018.

■ ACKNOWLEDGMENTS

DST (Project: YSS/2015/001552) supported the present research. S.S. acknowledges IIESTS, R.S. acknowledges RGNF, U.J. acknowledges DST-Inspire, S.D. acknowledges UGC for fellowship. Financial Support from IIESTS is duly acknowledged. We sincerely thank Asish Kr. Singha Deb, Scientific Officer, BARC, Trombay, Mumbai 400 085, India, for carrying out the ICPMS and ICPOES experiments. P.B. thanks CICECO-Aveiro Institute of Materials, POCI-01-0145-FEDER-007679 (FCT ref. UID/CTM/50011/2013), financed by national funds through the FCT/MEC and when appropriate cofinanced by FEDER under the PT2020 Partnership Agreement". V.S. and B.d.B. acknowledge support from the Research Priority Area Sustainable chemistry of the University of Amsterdam, and the Industrial Partnership Programme (IPP) Computational Sciences for Energy Research (project 13CSER003), which is financially supported by The Netherlands Organization for Scientific Research (NWO) and is cofinanced by Shell Global Solutions International B.V. The calculations were carried out on the Dutch national e-infrastructure with the support of the SURF cooperative. S.D. and F.M. thank the University of Göttingen for support. Use of the single crystal X-ray facility at SAIF-IIESTS is duly acknowledged.

■ DEDICATION

Dedicated in memory of Ms. Upasona Jash.

■ REFERENCES

(1) (a) Hili, R.; Yudin, A. K. Making Carbon-nitrogen Bonds in Biological and Chemical Synthesis. *Nat. Chem. Biol.* **2006**, *2*, 284−287. (b) Ullmann, F. Ueber eine neue bildungsweise von diphenylaminderivaten. *Ber. Dtsch. Chem. Ges.* **1903**, *36*, 2382−2384. (c) Goldberg, I. Ueber Phenylirungen Bei Gegenwart von Kupfer als Katalysator. *Ber. Dtsch. Chem. Ges.* **1906**, *39*, 1691−1692. (d) Barton, D. H. R.; Nakanishi, K.; Meth-Cohn, O. *Comprehensive Natural Products Chemistry*; Elsevier: Oxford, 1999; Vol. *4*. (e) Ricci, A. *Amino Group Chemistry, From Synthesis to the Life Sciences*; Wiley-VCH: Weinheim, 2007. (f) Bariwal, J.; Van der Eycken, E. C−N bond forming cross-coupling reactions: an overview. *Chem. Soc. Rev.* **2013**, *42*, 9283−9303. (g) Shin, K.; Kim, H.; Chang, S. Transition-Metal-Catalyzed C−N Bond Forming Reactions Using Organic Azides as the Nitrogen Source: A Journey for the Mild and Versatile C−H Amination. *Acc. Chem. Res.* **2015**, *48*, 1040−1052. (h) Park, Y.; Kim, Y.; Chang, S. Transition Metal-Catalyzed C−H Amination: Scope, Mechanism, and Applications. *Chem. Rev.* **2017**, *117*, 9247−9301.

(2) (a) Craig, P. N. *Comprehensive Medicinal Chemistry*; Drayton, C. J., Ed.; Pergamon Press: New York, 1991; Vol. *8*. (b) Cozzi, P.; Carganico, G.; Fusar, D.; Grossoni, M.; Menichincheri, M.; Pinciroli, V.; Tonani, R.; Vaghi, F.; Salvati, P. Imidazol-1-yl and pyridin-3-yl derivatives of 4-phenyl-1,4-dihydropyridines combining Ca^{2}+ antagonism and thromboxane A2 synthase inhibition. *J. Med. Chem.* **1993**, *36*, 2964−2972. (c) Katritzky, A. R.; Rees, C. W.; Scriven, E. F. V. *Comprehensive Heterocyclic Chemistry II*; Elsevier: Oxford, 1996. (d) Fairlamb, I. J. S. Regioselective (site-selective) Functionalisation of Unsaturated Halogenated Nitrogen, Oxygen and Sulfur Heterocycles by Pd-catalysed Cross-couplings and Direct Arylation Processes. *Chem. Soc. Rev.* **2007**, *36*, 1036−1045.

(3) (a) Ruiz-Castillo, P.; Buchwald, S. L. Applications of Palladium-Catalyzed C−N Cross-Coupling Reactions. *Chem. Rev.* **2016**, *116*, 12564−12649. (b) Ueda, S.; Su, M.; Buchwald, S. L. Completely N^{1}-Selective Palladium-Catalyzed Arylation of Unsymmetric Imidazoles: Application to the Synthesis of Nilotinib. *J. Am. Chem. Soc.* **2012**, *134*, 700−706. (c) Shuler, S. A.; Yin, G.; Krause, S. B.; Vesper, C. M.; Watson, D. A. Synthesis of Secondary Unsaturated Lactams via an Aza-Heck Reaction. *J. Am. Chem. Soc.* **2016**, *138*, 13830−13833. (d) Khatun, N.; Modi, A.; Ali, W.; Patel, B. K. Palladium-Catalyzed Synthesis of 2-Aryl-2*H*-Benzotriazoles from Azoarenes and $TMSN_3$. *J. Org. Chem.* **2015**, *80*, 9662−9670. (e) Zhou, Y.; Verkade, J. G. Highly Efficient Ligands for the Palladium-Assisted Double N-Arylation of Primary Amines for One-Sep Construction of Carbazoles. *Adv. Synth. Catal.* **2010**, *352*, 616−620. (f) Ikawa, T.; Barder, T. E.; Biscoe, M. R.; Buchwald, S. L. Pd-Catalyzed Amidations of Aryl Chlorides Using Monodentate Biaryl Phosphine Ligands: A Kinetic, Computational, and Synthetic Investigation. *J. Am. Chem. Soc.* **2007**, *129*, 13001−13007. (g) Hicks, J. D.; Hyde, A. M.; Cuezva, A. M.; Buchwald, S. L. Pd-Catalyzed N-Arylation of Secondary Acyclic Amides: Catalyst Development, Scope, and Computational Study. *J. Am. Chem. Soc.* **2009**, *131*, 16720−16734. (h) Beletskaya, I. P.; Cheprakov, A. V. The Complementary Competitors: Palladium and Copper in C−N Cross-Coupling Reactions. *Organometallics* **2012**, *31*, 7753−7808. (i) Vo, G. D.; Hartwig, J. F. Palladium-Catalyzed Coupling of Ammonia with Aryl Chlorides, Bromides, Iodides, and Sulfonates: A General Method for the Preparation of Primary Arylamines. *J. Am. Chem. Soc.* **2009**, *131*, 11049−11061. (j) Brusoe, A. T.; Hartwig, J. F. Palladium-Catalyzed Arylation of Fluoroalkylamines. *J. Am. Chem. Soc.* **2015**, *137*, 8460−8468. (k) Green, R. A.; Hartwig, J. F. Palladium-Catalyzed Amination of Aryl Chlorides and Bromides with Ammonium Salts. *Org. Lett.* **2014**, *16*, 4388−4391.

(4) (a) Wang, H.; Yu, Y.; Hong, X.; Tan, Q.; Xu, B. Rhodium-Catalyzed Direct *ortho* C−N Bond Formation of Aromatic Azo Compounds with Azides. *J. Org. Chem.* **2014**, *79*, 3279−3288. (b) Andersson, P. G.; Dauban, P.; Lescot, C.; Diaz-Requejo, M. M.; Perez, P. J. Rh-, Ag-, and Cu-Catalyzed C−N Bond Formation. *Innovative Catalysis in Organic Synthesis: Oxidation, Hydrogenation, and C-X Bond Forming Reactions*; Wiley, 2012. DOI: DOI: 10.1002/9783527646586.ch12. (c) Song, G.; Wang, F.; Li, X. C−C, C−O and C−N bond formation *via* rhodium(III)-catalyzed oxidative C−H activation. *Chem. Soc. Rev.* **2012**, *41*, 3651−3678. (d) Tang, C.; Yuan, Y.; Cui, Y.; Jiao, N. Rh-Catalyzed Diarylamine Synthesis by Intermolecular C−H Amination of Heteroarylarenes. *Eur. J. Org. Chem.* **2013**, *2013*, 7480−7483.

(5) (a) Yi, C. S. Recent Advances in the Synthetic and Mechanistic Aspects of the Ruthenium-Catalyzed Carbon-heteroatom Bond Forming Reactions of Alkenes and Alkynes. *J. Organomet. Chem.* **2011**, *696*, 76−80. (b) Ackermann, L.; Lygin, A. V.; Hofmann, N. Ruthenium-Catalyzed Oxidative Synthesis of 2-Pyridones through C−H/N−H Bond Functionalizations. *Org. Lett.* **2011**, *13*, 3278−3281. (c) Huang, L.; Arndt, M.; Gooßen, K.; Heydt, H.; Gooßen, L. Late Transition Metal-Catalyzed Hydroamination and Hydroamidation. *Chem. Rev.* **2015**, *115*, 2596−2697. (d) Arockiam, P. B.; Bruneau, C.; Dixneuf, P. H. Ruthenium(II)-Catalyzed C−H Bond Activation and Functionalization. *Chem. Rev.* **2012**, *112*, 5879−5918. (e) Utsunomiya, M.; Hartwig, J. F. Ruthenium-Catalyzed Anti-Markovnikov Hydroamination of Vinylarenes. *J. Am. Chem. Soc.* **2004**, *126*, 2702−2703. (f) Takemiya, A.; Hartwig, J. F. Rhodium-Catalyzed Intramolecular, Anti-MarkovnikovHydroamination. Synthesis of 3-Arylpiperidines. *J. Am. Chem. Soc.* **2006**, *128*, 6042−6043. (g) Wu, L.; Fleischer, I.; Jackstell, R.; Beller, M. Efficient and Regioselective Ruthenium-catalyzed Hydro-aminomethylation of Olefins. *J. Am. Chem. Soc.* **2013**, *135*, 3989−3996.

(6) (a) Antilla, J. C.; Klapars, A.; Buchwald, S. L. The Copper-Catalyzed *N*-Arylation of Indoles. *J. Am. Chem. Soc.* **2002**, *124*, 11684−11688. (b) Davis, O. A.; Hughes, M.; Bull, J. A. Copper-Catalyzed *N*-Arylation of 2-Imidazolines with Aryl Iodides. *J. Org. Chem.* **2013**, *78*, 3470−3475. (c) Kim, H.; Chang, S. Transition-Metal-Mediated Direct C−H Amination of Hydrocarbons with

DOI: 10.1021/acs.inorgchem.8b02877
Inorg. Chem. XXXX, XXX, XXX−XXX

Amine Reactants: The Most Desirable but Challenging C−N Bond-Formation Approach. *ACS Catal.* **2016**, *6*, 2341−2351. (d) Rasheed, S.; Rao, D. N.; Das, P. Copper-Catalyzed Inter- and Intramolecular C−N Bond Formation: Synthesis of Benzimidazole-Fused Heterocycles. *J. Org. Chem.* **2015**, *80*, 9321−9327. (e) Stabile, P.; Lamonica, A.; Ribecai, A.; Castoldi, D.; Guercio, G.; Curcuruto, O. Mild, convenient and versatile Cu-mediated synthesis of *N*-aryl-2-imidazolidinones. *Tetrahedron Lett.* **2010**, *51*, 3232−3235. (f) Hartwig, J. F. Evolution of a Fourth Generation Catalyst for the Amination and Thioetherification of Aryl Halides. *Acc. Chem. Res.* **2008**, *41*, 1534−1544. (g) Strieter, E. R.; Bhayana, B.; Buchwald, S. L. Mechanistic Studies on the Copper-Catalyzed *N*-Arylation of Amides. *J. Am. Chem. Soc.* **2009**, *131*, 78−88. (h) Zhu, L.; Cheng, L.; Zhang, Y.; Xie, R.; You, J. Highly Efficient Copper-Catalyzed *N*-Arylation of Nitrogen-Containing Heterocycles with Aryl and Heteroaryl Halides. *J. Org. Chem.* **2007**, *72*, 2737−2743. (i) Buchwald, S. L.; Bolm, C. On the Role of Metal Contaminants in Catalyses with $FeCl_3$. *Angew. Chem., Int. Ed.* **2009**, *48*, 5586−5587. (j) Larsson, P.-F.; Correa, A.; Carril, M.; Norrby, P.-O.; Bolm, C. Copper-Catalyzed Cross-Couplings with Part-per-Million Catalyst Loadings. *Angew. Chem., Int. Ed.* **2009**, *48*, 5691−5693. (k) Larsson, P.-F.; Bolm, C.; Norrby, P.-O. Kinetic Investigation of a Ligand-Accelerated Sub-mol% Copper-Catalyzed C-N Cross-Coupling Reaction. *Chem. - Eur. J.* **2010**, *16*, 13613−13616. (l) Larsson, P.-F.; Wallentin, C.-J.; Norrby, P.-O. Mechanistic Aspects of Submol% Copper-Catalyzed CN Cross-Coupling. *ChemCatChem* **2014**, *6*, 1277−1282. (m) Correa, A.; Bolm, C. Iron-Catalyzed N-Arylation of Nitrogen Nucleophiles. *Angew. Chem., Int. Ed.* **2007**, *46*, 8862−8865.

(7) (a) Ritleng, V.; Henrion, M.; Chetcuti, M. J. Nickel N-Heterocyclic Carbene-Catalyzed C−Heteroatom Bond Formation, Reduction, and Oxidation: Reactions and Mechanistic Aspects. *ACS Catal.* **2016**, *6*, 890−906. (b) Barker, T. J.; Jarvo, E. R. Umpolung Amination: Nickel-Catalyzed Coupling Reactions of *N*,*N*-Dialkyl-*N*-chloroamines with Diorganozinc Reagents. *J. Am. Chem. Soc.* **2009**, *131*, 15598−15599. (c) Ilies, L.; Matsubara, T.; Nakamura, E. Nickel-Catalyzed Synthesis of Diarylamines via Oxidatively Induced C−N Bond Formation at Room Temperature. *Org. Lett.* **2012**, *14*, 5570−5573. (d) Shimasaki, T.; Tobisu, M.; Chatani, N. Nickel-Catalyzed Amination of Aryl Pivalates by the Cleavage of Aryl C-O Bonds. *Angew. Chem., Int. Ed.* **2010**, *49*, 2929−2932. (e) Iglesias, M. J.; Prieto, A.; Nicasio, M. S. Well-Defined Allylnickel Chloride/N-Heterocyclic Carbene [(NHC)Ni(allyl)Cl] Complexes as Highly Active Precatalysts for C-N and C-S Cross-Coupling Reactions. *Adv. Synth. Catal.* **2010**, *352*, 1949−1954. (f) Rull, S. G.; Blandez, J. F.; Fructos, M. R.; Belderrain, T. R.; Nicasio, M. C. C-N Coupling of Indoles and Carbazoles with Aromatic Chlorides Catalyzed by a Single-Component NHC-Nickel(0) Precursor. *Adv. Synth. Catal.* **2015**, *357*, 907−911.

(8) (a) Chirik, P. J.; Wieghardt, K. Radical Ligands Confer Nobility on Base-metal Catalysts. *Science* **2010**, *327*, 794−795. (b) Broere, D. J. L.; Plessius, R.; van der Vlugt, J. I. New Avenues for Ligand-mediated Processes − Expanding Metal Reactivity by the use of Redox-active Catechol, *o*-Aminophenol and *o*-Phenylenediamine Ligands. *Chem. Soc. Rev.* **2015**, *44*, 6886−6915. (c) Luca, O. R.; Crabtree, R. H. Redox-active Ligands in Catalysis. *Chem. Soc. Rev.* **2013**, *42*, 1440−1459. (d) Lyaskovskyy, V.; de Bruin, B. Redox Non-Innocent Ligands: Versatile New Tools to Control Catalytic Reactions. *ACS Catal.* **2012**, *2*, 270−279. (e) de Bruin, B.; Gualco, P.; Paul, N. D. In *Ligand Design In Metal Chemistry: Reactivity and Catalysis*; Stradiotto, M., Lundgren, R., Eds.; Wiley: New York, 2015. (f) Smith, A. L.; Hardcastle, K. I.; Soper, J. D. Redox-Active Ligand-Mediated Oxidative Addition and Reductive Elimination at Square Planar Cobalt(III): Multielectron Reactions for Cross-Coupling. *J. Am. Chem. Soc.* **2010**, *132*, 14358−14360. (g) Sylvester, K. J.; Chirik, P. J. Iron-Catalyzed, Hydrogen-Mediated Reductive Cyclization of 1,6-Enynes and Diynes: Evidence for Bis(imino)pyridine Ligand Participation. *J. Am. Chem. Soc.* **2009**, *131*, 8772−8774. (h) Bouwkamp, M. W.; Bowman, A. C.; Lobkovsky, E.; Chirik, P. J. Iron-Catalyzed [$2\pi + 2\pi$] Cycloaddition of α,ω -Dienes: The Importance of Redox-Active Supporting Ligands. *J. Am. Chem. Soc.* **2006**, *128*, 13340−13341. (i) Yu, R. P.; Darmon, J. M.; Hoyt, J. M.; Margulieux, G. W.; Turner, Z. R.; Chirik, P. J. High-Activity Iron Catalysts for the Hydrogenation of Hindered, Unfunctionalized Alkenes. *ACS Catal.* **2012**, *2*, 1760−1764. (j) Huang, Y.; Moret, M.-E.; Klein Gebbink, R. J. M. Iron-Mediated Direct Arylation of Unactivated Arenes in Air. *Eur. J. Org. Chem.* **2014**, *2014*, 3788.

(9) (a) Schmidt, V. A.; Kennedy, C. R.; Bezdek, M. J.; Chirik, P. J. Selective [1,4]-Hydrovinylation of 1,3-Dienes with Unactivated Olefins Enabled by Iron Diimine Catalysts. *J. Am. Chem. Soc.* **2018**, *140*, 3443−3453. (b) Margulieux, G. W.; Bezdek, M. J.; Turner, Z. R.; Chirik, P. J. Ammonia Activation, H_2 Evolution and Nitride Formation from a Molybdenum Complex with a Chemically and Redox Noninnocent Ligand. *J. Am. Chem. Soc.* **2017**, *139*, 6110−6113. (c) Schaefer, B. A.; Margulieux, G. W.; Tiedemann, M. A.; Small, B. L.; Chirik, P. J. Synthesis and Electronic Structure of Iron Borate Betaine Complexes as a Route to Single-Component Iron Ethylene Oligomerization and Polymerization Catalysts. *Organometallics* **2015**, *34*, 5615−5623. (d) Chirik, P. J. Iron- and Cobalt-Catalyzed Alkene Hydrogenation: Catalysis with Both Redox-Active and Strong Field Ligands. *Acc. Chem. Res.* **2015**, *48*, 1687−1695. (e) Schmidt, V. A.; Hoyt, J. M.; Margulieux, G. W.; Chirik, P. J. Cobalt-Catalyzed [$2\pi + 2\pi$] Cycloadditions of Alkenes: Scope, Mechanism, and Elucidation of Electronic Structure of Catalytic Intermediates. *J. Am. Chem. Soc.* **2015**, *137*, 7903−7914.

(10) (a) Bagh, B.; Broere, D. L. J.; Sinha, V.; Kuijpers, P. F.; van Leest, N. P.; de Bruin, B.; Demeshko, S.; Siegler, M. A.; van der Vlugt, J. I. Catalytic Synthesis of N-Heterocycles via Direct C(sp^3)-H Amination using an Air-stable Iron(III) Species with a Redox-Active Ligand. *J. Am. Chem. Soc.* **2017**, *139*, 5117−5124. (b) Broere, D.; de Bruin, B.; Reek, J. N. H.; Lutz, M.; Dechert, S.; van der Vlugt, J. I. Intramolecular Redox-Active Ligand-to-Substrate Single Electron Transfer: Radical Reactivity with a Palladium(II) Complex. *J. Am. Chem. Soc.* **2014**, *136*, 11574−11577. (c) Smith, A. L.; Hardcastle, K. I.; Soper, J. D. Redox-Active Ligand-Mediated Oxidative Addition and Reductive Elimination at Square Planar Cobalt(III): Multielectron Reactions for Cross-Coupling. *J. Am. Chem. Soc.* **2010**, *132*, 14358−14360. (d) Blackmore, K. J.; Lal, N.; Ziller, J. W.; Heyduk, A. F. Catalytic Reactivity of a Zirconium(IV) Redox-Active Ligand Complex with 1,2-Diphenylhydrazine. *J. Am. Chem. Soc.* **2008**, *130*, 2728−2729. (e) Rhinehart, J. L.; Mitchell, N. E.; Long, B. K. Enhancing α-Diimine Catalysts for High-Temperature Ethylene Polymerization. *ACS Catal.* **2014**, *4*, 2501−2504. (f) Sikari, R.; Sinha, S.; Jash, U.; Das, S.; Brandaõ, P.; de Bruin, B.; Paul, N. D. Deprotonation Induced Ligand Oxidation in a Ni^{II} Complex of a Redox Noninnocent N1-(2-Aminophenyl)benzene-1,2-diamine and Its Use in Catalytic Alcohol Oxidation. *Inorg. Chem.* **2016**, *55*, 6114−6123.

(11) (a) te Grotenhuis, C.; van den Heuvel, N.; van der Vlugt, J. I.; de Bruin, B. Catalytic dibenzocyclooctene synthesis via cobalt(III)-carbene radical and ortho-quinodimethane intermediates. *Angew. Chem., Int. Ed.* **2018**, *57*, 140. (b) te Grotenhuis, C.; Das, B. G.; Kuijpers, P. F.; Hageman, W.; Trouwborst, M.; de Bruin, B. Catalytic 1,2-Dihydronaphthalene and *E*-Aryl-Diene Synthesis via Co^{III}-Carbene Radical and o-Quinodimethane Intermediates. *Chemical Science* **2017**, *8*, 8221−8230. (c) Das, B. G.; Chirila, A.; Tromp, M.; Reek, J. N. H; de Bruin, B. Co^{III}-Carbene Radical Approach to Substituted 1*H*-Indenes. *J. Am. Chem. Soc.* **2016**, *138*, 8968−8975. (d) Paul, N. D.; Mandal, S.; Otte, M.; Cui, X.; Zhang, X. P.; de Bruin, B. A. Metalloradical Approach to 2*H*-Chromenes. *J. Am. Chem. Soc.* **2014**, *136*, 1090−1096. (e) Paul, N. D.; Chirila, A.; Lu, H.; Zhang, X. P.; de Bruin, B. Carbene Radicals in Cobalt(II) Porphyrin-Catalysed Carbene Carbonylation Reactions; A Catalytic Approach to Ketenes. *Chem. - Eur. J.* **2013**, *19*, 12953−12958.

(12) (a) Sarkar, B.; Kaim, W.; Fiedler, J.; Duboc, C. Molecule-Bridged Mixed-Valent Intermediates Involving the Ru^{I} Oxidation State. *J. Am. Chem. Soc.* **2004**, *126*, 14706−14707. (b) Frantz, S.; Hartmann, H.; Doslik, N.; Wanner, M.; Kaim, W.; Kümmerer, H.; Denninger, G.; Barra, A.; Duboc-Toia, C.; Fiedler, J.; Ciofini, I.;

DOI: 10.1021/acs.inorgchem.8b02877
Inorg. Chem. XXXX, XXX, XXX−XXX

Urban, C.; Kaupp, M. Multifrequency EPR Study and Density Functional g-Tensor Calculations of Persistent Organorhenium Radical Complexes. *J. Am. Chem. Soc.* **2002**, *124*, 10563−10571. (c) Doslik, N.; Sixt, T.; Kaim, W. The First Structural Characterization of an Azoaromatic Radical Anion Stabilized by Dicopper(I) Coordination. *Angew. Chem., Int. Ed.* **1998**, *37*, 2403−2404. (d) Shivakumar, M.; Pramanik, K.; Ghosh, P.; Chakravorty, A. Isolation and Structure of the First Azo Anion Radical Complexes of Ruthenium. *Inorg. Chem.* **1998**, *37*, 5968−5969. (e) Sengupta, D.; Ghosh, P.; Chatterjee, T.; Datta, H.; Paul, N. D.; Goswami, S. Ligand-Centered Redox in Nickel(II) Complexes of 2-(Arylazo)pyridine and Isolation of 2-Pyridyl-Substituted Triaryl Hydrazines via Catalytic N-Arylation of Azo-Function. *Inorg. Chem.* **2014**, *53*, 12002−12013. (f) Joy, S.; Krämer, T.; Paul, N. D.; Banerjee, P.; McGrady, J. E.; Goswami, S. Isolation and Assessment of the Molecular and Electronic Structures of Azo-Anion-Radical Complexes of Chromium and Molybdenum. Experimental and Theoretical Characterization of Complete Electron-Transfer Series. *Inorg. Chem.* **2011**, *50*, 9993−10004. (g) Paul, N. D.; Samanta, S.; Goswami, S. Redox Induced Electron Transfer in Doublet Azo-Anion Diradical Rhenium(II) Complexes. Characterization of Complete Electron Transfer Series. *Inorg. Chem.* **2010**, *49*, 2649−2655. (h) Paul, N. D.; Samanta, S.; Mondal, T. K.; Goswami, S. Examples of Reductive Azo Cleavage and Oxidative Azo Bond Formation on $Re_2(CO)_{10}$ Template: Isolation and Characterization of Re(III) Complexes of New Azo-Aromatic Ligands. *Inorg. Chem.* **2011**, *50*, 7886−7893. (i) Paul, N. D.; Krämer, T.; McGrady, J. E.; Goswami, S. Dioxygen Activation by Mixed-valent Dirhodium Complexes of Redox Non-innocent Azoaromatic Ligands. *Chem. Commun.* **2010**, *46*, 7124−7126.

(13) (a) Sengupta, D.; Bhattacharjee, R.; Pramanick, R.; Rath, S. P.; Saha Chowdhury, N.; Datta, A.; Goswami, S. Exclusively Ligand-Mediated Catalytic Dehydrogenation of Alcohols. *Inorg. Chem.* **2016**, *55*, 9602−9610. (b) Pramanick, R.; Bhattacharjee, R.; Sengupta, D.; Datta, A.; Goswami, S. An Azoaromatic Ligand as Four Electron Four Proton Reservoir: Catalytic Dehydrogenation of Alcohols by Its Zinc(II) Complex. *Inorg. Chem.* **2018**, *57*, 6816.

(14) (a) Sinha, S.; Das, S.; Sikari, R.; Parua, S.; Brandaõ, P.; Demeshko, S.; Meyer, F.; Paul, N. D. Redox Noninnocent Azo-Aromatic Pincers and Their Iron Complexes. Isolation, Characterization, and Catalytic Alcohol Oxidation. *Inorg. Chem.* **2017**, *56*, 14084−14100. (b) Das, S.; Sinha, S.; Jash, U.; Sikari, R.; Saha, A.; Barman, S. K.; Brandão, P.; Paul, N. D. Redox-Induced Interconversion and Ligand-Centered Hemilability in Ni(II) Complexes of Redox-Noninnocent Azo-Aromatic Pincers. *Inorg. Chem.* **2018**, *57*, 5830−5841.

(15) (a) Barham, J. P.; Coulthard, G.; Emery, K. J.; Doni, E.; Cumine, F.; Nocera, G.; John, M. P.; Berlouis, L. E. A.; McGuire, T.; Tuttle, T.; Murphy, J. A. KO^{t}Bu: A Privileged Reagent for Electron Transfer Reactions? *J. Am. Chem. Soc.* **2016**, *138*, 7402−7410. (b) Yi, H.; Jutand, A.; Lei, A. Evidence for the Interaction Between ^{t}BuOK and 1,10-Phenanthroline to form the 1,10-Phenanthroline Radical Anion: a Key Step for the Activation of Aryl Bromides by Electron Transfer. *Chem. Commun.* **2015**, *51*, 545−548. (c) Cuthbertson, J.; Gray, V. J.; Wilden, J. D. Observations on Transition Metal Free Biaryl Coupling: Potassium tert-Butoxide Alone Promotes the Reaction without Diamine or Phenanthroline Catalysts. *Chem. Commun.* **2014**, *50*, 2575−2578.

(16) (a) Das, C.; Ghosh, A. K.; Hung, C.-H.; Lee, G.-H.; Peng, S.-M.; Goswami, S. Metal-Promoted Aromatic Ring Amination and Deamination Reactions at a Diazo Ligand Coordinated to Rhodium and Ruthenium. *Inorg. Chem.* **2002**, *41*, 7125−7135. (b) Das, C.; Saha, A.; Hung, C.-H.; Lee, G.-H.; Peng, S.-M.; Goswami, S. Ruthenium Complexes of 2-[(4-(Arylamino)phenyl)azo]pyridine Formed via Regioselective Phenyl Ring Amination of Coordinated 2-(Phenylazo)pyridine: Isolation of Products, X-ray Structure, and Redox and Optical Properties. *Inorg. Chem.* **2003**, *42*, 198−204. (c) Kamar, K. K.; Das, S.; Hung, C.-H.; Castiñeiras, A.; Kuz'min, M. D.; Rillo, K. C.; Bartolomé, J.; Goswami, S. Design and Synthesis of a New Binucleating Ligand via Cobalt-Promoted C−N Bond Fusion Reaction. Ligand Isolation and Its Coordination to Nickel, Palladium, and Platinum. *Inorg. Chem.* **2003**, *42*, 5367−5375.

(17) The DFT barriers obtained at the BP86, def2-TZVP DFT-D3 level are rather low and do not explain the elevated temperatures needed in the experimental reactions. There can be several reasons for the need for elevated temperatures in the experimental catalytic reactions such as the presence of (lower energy) dormant species that were not explored computationally. The computational barriers might also be somewhat underestimated. Higher level calculations (using, e.g., meta-GGA functionals) could perhaps lead to somewhat higher barriers. However, exploring these possibilities is beyond the scope of the present paper.

(18) For nucleophiles where only one nitrogen center is available, the reaction will definitely go through the nitrogen that is bound to the iron center.

(19) *Bruker SAINT-plus*; Bruker AXS Inc.: Madison, WI, 2007.

(20) (a) Sheldrick, G. M. *SHELXS-97, A Program for Crystal Structure Solution*; University of Göttingen: Göttingen, Germany, 1997. (b) Sheldrick, G. M. *SHELXL-97, a Program for Crystal Structure Refinement*; University of Göttingen: Göttingen, Germany, 1997.

(21) Sheldrick, G. M. A short history of SHELX. *Acta Crystallogr., Sect. A: Found. Crystallogr.* **2008**, *A64*, 112−122.

(22) Ahlrichs, R. *Turbomole Version 6.5*; Theoretical Chemistry Group, University of Karlsruhe, 2013.

(23) PQS version 2.4, 2001, Parallel Quantum Solutions, Fayettevile, Arkansas (USA); the Baker optimizer is available separately from PQS upon request: Baker, I. *J. Comput. Chem.* **1986**, *7*, 385.

(24) Budzelaar, P. H. M. *J. Comput. Chem.* **2007**, *28*, 2226.

(25) (a) Becke, A. D. Density-functional exchange-energy approximation with correct asymptotic behavior. *Phys. Rev. A: At., Mol., Opt. Phys.* **1988**, *38*, 3098−3100. (b) Perdew, J. P. Density-functional approximation for the correlation energy of the inhomogeneous electron gas. *Phys. Rev. B: Condens. Matter Mater. Phys.* **1986**, *33*, 8822−8824.

(26) Sierka, M.; Hogekamp, A.; Ahlrichs, R. Fast evaluation of the Coulomb potential for electron densities using multipole accelerated resolution of identity approximation. *J. Chem. Phys.* **2003**, *118*, 9136−9148.

(27) Schaefer, A.; Horn, H.; Ahlrichs, R. Fully optimized contracted Gaussian basis sets for atoms Li to Kr. *J. Chem. Phys.* **1992**, *97*, 2571−2577.

(28) Grimme, S.; Antony, J.; Ehrlich, S.; Krieg, H. A consistent and accurate ab initio parametrization of density functional dispersion correction (DFT-D) for the 94 elements H-Pu. *J. Chem. Phys.* **2010**, *132* (154104), 1−19.

(29) Dzik, W. I.; Xu, X.; Zhang, X. P.; Reek, J. N. H.; de Bruin, B. 'Carbene Radicals' in Co^{II}(por)-Catalyzed Olefin Cyclopropanation. *J. Am. Chem. Soc.* **2010**, *132*, 10891−10902.

DOI: 10.1021/acs.inorgchem.8b02877
Inorg. Chem. XXXX, XXX, XXX−XXX